Conserved degronome features governing quality control-associated proteolysis

Bayan Mashahreh[1], Shir Armony[1], Kristoffer Enøe Johansson[3], Alon Chapelbaum[1], Nir Friedman[1], Richard G. Gardner[2], Rasmus Hartmann-Petersen[3], Kresten Lindorff-Larsen[3], Tommer Ravid[1*]

[1]Department of Biological Chemistry, The Alexander Silberman Institute of Life Sciences, The Hebrew University of Jerusalem, Jerusalem, Israel

[2]Department of Pharmacology, University of Washington, Seattle, WA 98195, USA

[3]The Linderstrøm-Lang Centre for Protein Science, Department of Biology, University of Copenhagen, Copenhagen, Denmark

*Correspondence: tommer.ravid@mail.huji.ac.il

Summary

The eukaryotic proteome undergoes constant surveillance by quality control systems that either sequester, refold, or eliminate aberrant proteins by ubiquitin-dependent mechanisms. Ubiquitin-conjugation necessitates the recognition of degradation determinants, termed degrons, by their cognate E3 ubiquitin-protein ligases. To learn about the distinctive properties of quality control degrons, we performed an unbiased peptidome stability screen in yeast. The search identified a large cohort of proteome-derived degrons., some of which exhibited broad E3 ligase specificity. Consequent application of a machine-learning algorithm established constraints governing degron potency, including the amino acids composition and secondary structure propensities. According to the set criteria, degrons with transmembrane domain-like characteristics are the most probable sequences to act as degrons. Similar quality control degrons were identified in viral and human proteins, suggesting for conserved degradation mechanisms. Altogether, the emerging data indicate that transmembrane domain-like degron features have been preserved in evolution as key quality control determinants of proteins' half-life.

Keywords: Protein Quality Control, Quality Control Associated Proteolysis, Ubiquitin-Proteasome System, degrons, Global Protein Stability, Protein Stability Index, peptidome, degronome.

Introduction

Intracellular protein quality control (PQC) is a principal regulatory mechanism for the maintenance of protein homeostasis (Balchin et al., 2016). PQC systems continuously survey the proteome and execute a triage of unfolded protein states, the result of which is either refolding or, if beyond repair, either sequestration or degradation of aberrant proteins (Kästle and Grune, 2012; Shiber and Ravid, 2014). Protein refolding and sequestration are primarily mediated by molecular chaperones (Kim et al., 2013; Sontag et al., 2017; Tyedmers et al., 2010), while the Ubiquitin-Proteasome System (UPS) executes quality control-associated proteolysis (QCAP) (Amm et al., 2014).

Key to understanding protein homeostasis is deciphering the mode by which QCAP pathways discern the folding state of proteins. It has been established that the ubiquitin conjugation system, via E3 ubiquitin-protein ligases and auxiliary chaperones, recognizes degradation determinants termed degrons (Varshavsky, 1991) that constitute inherent sequences and structural features, as well as acquired post-translational modifications (Guharoy et al., 2016). To date, degrons have been mostly identified through studies of regulated protein degradation mechanisms, such as those involved in cell division and differentiation, as well as in many cancer-related diseases (Koliopoulos and Alfieri, 2021; Mészáros et al., 2017; Rape, 2018). These studies identified inherent degrons as short motifs, such as the destruction box of cyclins, as well as acquired degrons that are activated by phosphorylation or other post-translational modifications (Ang and Wade Harper, 2005; Davey and Morgan, 2016; Filipčík et al., 2017; Lucas and Ciulli, 2017). However,

the repertoire of known degrons cannot explain the large diversity in half-lives exhibited by the proteome (Christiano et al., 2014; Eden et al., 2011).

Our earlier work exposed the large sequence heterogenicity of the cellular degron landscape (degronome) in yeast, which led to the proposition that the majority of the eukaryotic proteome contains cryptic QCAP degrons that may become exposed naturally or under misfolding conditions, such as cellular and environmental stresses (Ella et al., 2019; Geffen et al., 2016). These degrons target protein ubiquitination via the activity of a relatively small number of designated QCAP E3 ligases, suggesting that each recognizes a large set of substrates (Breckel and Hochstrasser, 2021). Furthermore, QCAP E3 enzymes can act redundantly in the ubiquitination of their substrates, seemingly exhibiting overlapping recognition mechanisms (Hickey et al., 2021; Maurer et al., 2016; Samant et al., 2018). However, the significance of this functional redundancy is not yet fully understood.

Here we describe a yeast-adapted Global Protein Stability (GPS)-peptidome technology (yGPS-P) originally established for the discovery of degrons in mammalian cell lines (Koren et al., 2018; Lin et al., 2018; Yen et al., 2008). By employing a peptide library fused to yGPS-P, we have identified multiple degron sequences that were subsequently analyzed using a machine learning algorithm. The resulting computer program, termed Quality Control Degron Prediction (QCDPred)(Johansson et al., submitted), revealed amino acid and secondary structure preferences in QCAP degrons. The determined degron features were highly dependent on the overall hydrophobicity, and consistently transmembrane domains (TMDs) exhibit extreme degron potency, signifying their critical role in the degradation of integral membrane proteins prevented from entering the secretory pathway.

Results

Yeast-based GPS-peptidome technology

To set up a comprehensive degron discovery platform in the yeast *Saccharomyces cerevisiae* proteome, we applied a fluorescence-based GPS technology (Yen et al., 2008), previously developed in cultured human cells (Koren et al., 2018; Lin et al., 2018). yGPS-P utilizes a bicistronic gene expression system in which codon-optimized versions of yeast enhanced Cherry and yeast enhanced GFP are expressed from a single transcript. Yet, the two proteins are translated separately due to the presence of an Internal Ribosome Entry Site (IRES) upstream to GFP that allows translation initiation in a cap-independent manner (Edwards and Wandless, 2010) (Figure 1A). A yeast GPS peptidome library (yGPS-P_{lib}) is generated by subsequent in-frame insertion of proteome-derived DNA fragments downstream to GFP in a yGPS-P vector (Figure 1A). The plasmid library is transformed into yeast, followed by quantitative flow cytometry or Fluorescence-Activated Cell Sorting (FACS) (Figure 1B). As both Cherry and GFP are expressed from a single transcript yet translated independently, Cherry levels reflect the basal expression of the reporters while the ratio between GFP to Cherry (shown henceforth as yeG/yeC) determines the relative GFP protein level that is governed by the fused peptide.

To validate the use of yGPS-P as a degron discovery platform, we examined the competence of two well-characterized QCAP degrons of the Doa10 E3 ligase, *CL1* and *DegAB* (Alfassy et al., 2013; Furth et al., 2011; Gilon et al., 1998, 2000) to trigger degradation of the otherwise stable GFP. Doa10 is an endoplasmic reticulum (ER)-embedded enzyme that operates in ER-associated degradation (ERAD) (McCracken and Brodsky, 1996; Swanson et al., 2001). When the yeG/yeC ratio in cells expressing the fused degrons was compared to empty vector control, more than 5-fold decrease was observed, presumably due to UPS-mediated proteolysis (Figure 1C, *upper panel*). An increase in yeG/yeC in *doa10*Δ cells confirmed this assertion. That the increase in

yeG/yeC is indeed a result of elevated GFP protein levels was demonstrated by immunoblot analysis of the corresponding fusion proteins (Figure 1C, *lower panel*).

As a source for a peptide library, we chose a subset of proteins, all components of multimeric protein complexes that potentially undergo QCAP triage (Padovani et al., 2022). In total, 335 yeast proteins that are part of 23 different complexes were selected (Supplemental Table 1). Consequently, 51-mer DNA fragments with 36-mer DNA overlaps (corresponding to 17 amino acid-length tiled peptides with 12 amino acid overlaps) were synthesized to give rise to yGPS-P_{lib} (library) containing approximately 29,500 DNA fragments. yGPS-P_{lib} was transformed into yeast, followed by flow cytometry determination of the yeG/yeC ratio. The observed decrease in yeG/yeC in yGPS-P_{lib} (Figure 1D) indicates the presence of a destabilizing peptide population within the tested peptidome. To assess the contribution of degrons of the UPS to GFP destabilization, the effect of the irreversible proteasome inhibitor Bortezomib (BZ) on yeG/yeC was determined. To this end, yGPS-P_{lib} was transformed into cells lacking the multidrug transporter *PDR5 (pdr5*Δ) to increase drug sensitivity (Leppert et al., 1990). Comparing mock- and drug-treated cells, we observed an increase in the overall cellular levels of ubiquitin conjugates (confirming proteasome inhibition), as well as a mild increase in yeG/yeC (Figure 1E, *left & middle panels*). A larger increase of yeG/yeC was observed when a pre-sorted top 10% degron-enriched population was tested (Fig. 1E, *right panel* and Supplemental Figure 1), confirming that changes in yeG/yeC accurately reflect susceptibility to UPS-mediated degradation.

Amino acid classification of QCAP degrons

To classify degron sequences within yGPS-P_{lib}, mid-log-phase cells expressing the appended peptidome were separated by FACS into four gates according to yeG/yeC, each containing an equal cell number, and the identity and amounts of peptides DNA in the different gates were

determined by Next-Generation Sequencing (NGS) (Figure 2A). After filtering ambiguous peptides DNA from the NGS data, the contribution of 23,600 peptides to GFP stability was calculated based on their abundance in the different gates and each was assigned a Protein Stability Index (PSI) (Yen et al., 2008)(Figure 2A and Supplemental Table 2). Overall, 9.5% of the analyzed peptidome had PSI values < 1.7 (on a scale of 1 – 4).

Employing various search tools, we could not observe linear amino acid sequence motifs or C-terminal amino acid preferences within the examined degrons, (see also Geffen et al., 2016). We therefore opted to identify differences in the amino acid distribution within the recovered peptidome, which was separated into six bins according to their PSI values (Figure 2B), and the absolute and relative abundance of amino acid residues in peptides within each bin were determined (Figure 2C, *left and right panels*, respectively). Most amino acids constituting the library peptidome were arbitrarily distributed between the different bins. However, leucine and isoleucine and to lesser extent phenylalanine and tyrosine were significantly enriched in bin1, and their levels gradually decline in the following (more stable) bins. Conversely, levels of the two negatively charged amino acids, glutamate and aspartate, and to a lesser extent glycine were least represented in bin1 and were enriched in the following bins. These findings imply that the presence of negatively charged amino acids specifically interferes with a QCAP degron's function. This was confirmed by replacing three amino acids with either glutamate or arginine in a re-evaluated proteasome-dependent degron peptide P3 from the yeast protein Qcr9 (Figures 2D, 2E, See Oligos Table in "Materials and Methods"). We concluded that the classified QCAP degronome prefers branched-chain and bulky hydrophobic residues while negatively charged amino acids are disfavored.

We next examined these assertions on a native QCAP degron from the P-type Cation-transporting ATPase Pca1, that was not in our tested degron cohort. Under standard growth conditions, Pca1 is constitutively degraded via Doa10, which recognizes a cysteine enriched degron localized within amino acids 271-320 of the cytosolic and solvent-exposed N-terminal region of Pca1 (Adle and Lee, 2008; Smith et al., 2016). However, cadmium sensing by the degron enables Pca1 to circumvent ERAD (Adle and Lee, 2008). As this region is too long for precise analysis, we located a shorter sequence that defines the operational degron, using QCDPred, a machine-learning algorithm we have developed by using the PSI data to train a logistic regression model (Johansson et al, submitted). Consistent with previous findings (Smith et al., 2016), QCDPred identified a destabilizing element between amino acids 289-305, which was predicted by AlphaFold (Jumper et al., 2021; Varadi et al., 2022) to form an exposed helix-turn-helix structure (Figure 2F). Examining Pca1 steady-state levels, we observed that replacing three amino acids in the degron core (Figure 2F) with aspartate residues greatly stabilized the protein (Figure 2G). Conversely, replacing the same amino acids with arginine residues only showed moderate stabilization (Figure 2G). Importantly, mutant Pca1 still retained cadmium sensitivity (Figure 2G), indicating overall structural preservation. These data confirmed our assertion that negatively charged amino acids greatly interfere with native QCAP degron's function. The data also demonstrated the capability of QCDPred to identify functional degrons within the proteome while in their physiological context. Consequently, protein stability maps were formed for all proteins comprising the tested library that attained 100% coverage (N=306), each includes experimental PSI values for each peptide, average PSI values for each amino acid, and QCDPred probability scores (Supplemental Table 3 and Supplemental Figure 2).

Transmembrane domains function as QCAP degrons

Intriguingly, besides the aforementioned cytosolic degron, QCDPred also assigned remarkably high degron probabilities ($P \geq 0.93$) to Pca1 TMDs (Figure 3A). This was unexpected, not only because QCDPred was not programmed to consider protein topology, but also because TM proteins comprised only a minute proportion of the proteins included in the screen (1.79%) and hence their small contribution to the algorithm. The observation is perfectly in line with PQC degrons being hydrophobic (Figure 2C). Thus, when applying QCDPred to the entire yeast proteome, the vast majority of TMDs were assigned as degrons (Figure 3B). Our experimental peptidome data agree with this prediction, demonstrating that 12 out of 13 peptides localized to TMDs of the inner mitochondrial cytochrome b-c1 respiratory complex (Trumpower, 1990), the only TM-embedded complex in our peptidome cohort (Supplemental Table 1), function as degrons (Figure 3C and Supplemental Figure 3). In line with these findings, most predicted TMD degrons in the yeast proteome were enriched in the highest QCDPred score range of 0.95-1.0 while the rest of the degrons were underrepresented in this range (Figure 3D). Thus, according to QCDPred, TMDs comprise the most potent QCAP degron sequences. Hence, the hydrophobic sequence and possibly structural resemblance to TMDs is likely a significant feature of QCAP degrons. TMDs themselves could be relevant as PQC degrons in cases when TM proteins fail to insert correctly in membranes (see next).

Since the QCDPred algorithm is based on data from short peptides and thereby devoid of the cellular context, we wished to empirically assess the putative function of TMDs as potential degrons in a more physiological setting. To this end, three single-pass type-I proteins were selected to examine our hypothesis. These include the COPII-coated vesicles protein Erp2 (Marzioch et al., 1999), Atg27, which is involved in autophagy and coated-vesicle transport (Yen et al., 2007), and Ksh1 which functions in the early steps of the secretory pathway (Wendler et al., 2010). When

expressed as GFP fusions, all three proteins exhibited membrane enrichment (Figure 4A). QCDPred assigned degron function to both the N-terminal signal peptides (SPs) that mediate ER insertion (Hegde and Keenan, 2022) and the TMDs of the three proteins (Figures 4B). This was confirmed experimentally by fusing either the TM or SP regions of the three proteins C-terminally to GFP (a position that is unlikely to support ER translocation), followed by flow cytometry analysis (Figures 4C, 4D). Thus, besides ER targeting, SPs may additionally function as QCAP degrons if translocation fails.

As the removal of the SP would likely disrupt ER targeting, we hypothesized that this would in turn lead to a rapid turnover of TMD-containing proteins via recognition of TM regions as degrons. This was tested by determining the steady-state levels, with or without the SP, of Erp2, Atg27, and Ksh1 (Figure 4E, Supplemental Figure 4). Appending the full-length proteins N-terminally to GFP resulted in partial destabilization, assumingly by QCAP, that indeed, was greatly enhanced by the removal of the SP. Curiously, $_{\Delta SP}$Atg27 did not respond to proteasome inhibition while levels of $_{\Delta SP}$Erp2 and $_{\Delta SP}$Ksh1 were significantly increased (Supplemental Figure 4), suggesting a proteasome-independent degradation mechanism for the mislocalized autophagy-associated protein. Notably, positioning of the cytosolic exposed degrons is immaterial to their function as both N-terminally- and C-terminally-appended SP-excluded proteins were substantially unstable. (Figures 4E, 4F).

<u>QCAP degron characteristics</u>

The data so far indicate that in the yeast proteome QCAP degrons are widespread and that these regions are prevalent in hydrophobic residues while negatively charged residues are scarce. This leads to the question as to whether sequence hydrophobicity is the defining factor for a QCAP degron's function. As expected from the parameters that are used in QCDPred, the average

QCDPred scores of most amino acid types are correlated with their Kyte-Doolittle hydrophobicity scores (Figure 5A) and, indeed, all hydrophobic amino acids contribute positively to QCAP degrons' probability. Nevertheless, within hydrophobic degrons there is a bias for particular residues (Supplemental figure 5): Comparing the distribution of amino acids in hydrophobic TMD protein regions with high degron probability, to a small set of TMDs with lower degron probability revealed that the former is enriched in bulky and branched hydrophobic amino acids, while the latter express small hydrophobic amino acids instead (Supplemental figure 5). In addition, we identified a prevalence for alpha-helical configurations in QCAP degrons when found in their native context (Figure 5B) that not only agrees with the established helical structure of TMDs but also correlates strongly with increased non-TMD degron probabilities (Figure 5C). Interestingly, PQC degrons were hardly found in N/A (not assigned) regions that are likely disordered (Figure 5B). This implies that for most PQC degrons to become active, the protein must be structurally perturbed so that the degron is exposed. Indeed, we have found that for disordered proteins and regions there is a correlation between the presence of predicted degrons and the abundance and half-lives of the proteins (Johansson et al, submitted). Altogether, our data indicate that QCAP degrons are enriched in bulky hydrophobic TMD-like entities.

We next tested whether the linear order of amino acids within a degron determines its function. To this end, the amino acid sequence of a peptide P1 from the yeast protein COB of the b-c1 complex was scrambled to form two random peptides having identical amino acid content, hence also identical degron probability. When fused to the C-terminus of GFP, all three peptides were predicted to form helices, yet to various degrees (Supplemental Figure 6). Both scrambled peptides not only conferred GFP degradation but were even more potent than the original P1 peptide,

indicating that the general chemical properties of the degron, rather than its exact linear sequence is a principal QCAP degron determinant (Figure 5D).

Degrons presence correlates with proteins function

We next searched for roles governing the distribution of degrons in the proteome. Specifically, whether it is simply dependent on the probability of finding a specific sequence within the entire proteome or associated with specific protein property or function. As shown in Figure 5E, a weak monotonic relation was observed between protein length and degron presence (Spearman rank correlation coefficient (ρ) of 0.46), thus excluding random distribution of the predicted QCAP degronome. We then analyzed degrons through Gene Ontology (GO) annotation (Figure 5F). To this end, the yeast proteome was classified, based on QCDPred score into two groups- one with and one without degrons at high significance ($P \geq$ or < 0.85). Each group was then used as input for determining GO processes using the Saccharomyces Genome Database (SGD) Gene Ontology Slim Term Mapper (https://www.yeastgenome.org/goSlimMapper). Data in Figure 5F and Supplemental Figure 7 show that proteins engaged in transport and lipid metabolism are enriched in QCAP degrons. Many of these protein classes are integrated into membranes, an observation that agrees with our finding that TMDs can also act as QCAP degrons when exposed to the PQC system. Conversely, proteins, where QCAP degrons are underrepresented, are mostly involved in transcription, translation, ribosome assembly, as well as protein folding. The latter group is of particular interest as it implies that the exclusion of QCAP degrons in chaperones involved in proteolysis renders them resistant to degradation themselves. Indeed, QCDPred analysis of a collection of cytosolic/nuclear yeast chaperones predicted one or more degrons in Hsp90, Hsp104, and Hsp110 family members, while Hsp40 and Hsp70 family members, that are directly involved

in proteolysis (Shiber and Ravid, 2014), were mostly devoid of QCAP degrons (Supplemental Figure 8).

Partial selectivity of QCAP E3 ligases

To learn about UPS-dependent QCAP functionality, we next examined degron specificity of Ubiquitin-protein E3 ligases. To this end, the aforementioned peptide library was inserted into yeast strains lacking one of three well-defined QCAP E3 ligases – Doa10, which is a multi-TMDs E3 ligase that localizes to the outer leaflet of the ER membrane and the nuclear envelope (Deng and Hochstrasser, 2006), Ubr1, which is a soluble protein residing in the cytoplasm and the nucleoplasm (Prasad et al., 2018), and San1, which is exclusively nuclear E3 (Gardner et al., 2005). yGPS-P_{lib} transformation into E3 deleted (*E3*Δ) strains was followed by FACS and NGS, and PSI scores of degrons having $P < 1.7$ were determined and compared to that of *pdr5*Δ cells that served as a control strain (Supplemental Table 2). All knockout groups displayed a significant increase in degrons PSI scores (Kruskal-Wallis test $P < 0.001$). A Venn diagram determining E3 functional overlaps indicates that approximately one third of degrons were recognized by two or more E3 enzymes (Figure 5G). This finding is consistent with that of Hickey and colleagues who showed distinct yet overlapping QCAP E3 ligases substrate specificity governed by E3 subcellular localization (Hickey et al., 2021).

Conserved constraints governing degron potency

Considering the high conservation of QCAP pathways in the evolution of all eukaryotes, we hypothesized that QCAP degron properties are similarly well preserved. To test this paradigm, we next investigated how well the yeast-based QCDPred algorithm predicts the presence of QCAP degrons in other organisms and selected the influenza C virus p42 protein and human serum and

glucocorticoid-inducible kinase 1 (SGK1) as test cases. The influenza p42 contains a signal peptidase site at residue 259 that upon cleavage yields the p31 and CM2 proteins (Figure 6A, *upper panel*). CM2 integrates into the ER membrane through a single TMD, while p31 is rapidly degraded by the UPS via a degron at the C-terminal region (Pekosz and Lamb, 2000). As anticipated, both the C-terminal region of p31 and the TMD of p42 were predicted by QCDPred to function as degrons (Figure 6A, *lower panel*), however, during viral infection only the C-terminal region of p31 likely functions as a degron because it is accessible to the degradation system. Furthermore, Arteaga and co-workers have previously demonstrated that an amphipathic helix at the N-terminus of SGK1 targets the protein for proteolysis (Arteaga et al., 2006). Indeed, QCDPred analysis of SGK1 revealed three potential degrons, the strongest of which is placed between amino acids 17 and 29, the same region that was previously identified as a QCAP degron (Arteaga et al., 2006) (Figure 6B).

Having demonstrated that the tested non-yeast QCAP degrons can be predicted by QCDPred, we next wanted to investigate the universality of QCAP degrons by testing whether the principles established for yeast degrons generally apply to the human degronome. To this end, we assessed the correlation between PSI values, previously assigned for C-terminal regions of the entire human proteome (Koren et al., 2018), and their average QCDPred probabilities. The comparison yielded a high correlation ($\rho = -0.74$) (Figure 6C), similar to that observed for the yeast N-terminome ($\rho = -0.78$) (Kats et al., 2018)(Figure 6D), indicating that indeed the principles of QCAP degron features are evolutionarily conserved. Consequently, average QCDPred scores were assigned to each amino acid in both the yeast and human proteomes (Supplemental Tables 4,5) and we provide QCDPred as a general tool to predict degrons in proteins present in the UniProt database (Johansson et al., submitted).

Discussion

The discovery that E3 ligases selectively bind substrates through recognition of distinct determinants (degrons) established their role as substrate recognition modules of the UPS (Hershko et al., 1986). Consequently, the identification of degrons has become one of the focal points of the UPS research. Initially, the hunt for degrons identified mostly acquired determinants that are, for example, the result of transient post-translational modifications such as phosphorylation that induce timely, regulated degradation via dedicated E3 ligases (Zheng and Shabek, 2017). Obviously, acquired degrons do not account for the majority of QCAP, carried out by specialized E3 ligase systems that monitor proteins folding state, presumably recognizing internal sequences that may become exposed following conformational aberrations. This assertion was confirmed during the characterization of *Deg1* degron of the Doa10 E3 ligase (Hochstrasser and Varshavsky, 1990; Swanson et al., 2001). *Deg1* is masked in the Mata1/Mat α2 mating-type dimer and exposed upon complex dissociation (Johnson et al., 1998). Critical for *Deg1* degron function is an amphipathic helix (Johnson et al., 1998), also present in other synthetic and authentic Doa10 substrates (Arteaga et al., 2006; Furth et al., 2011; Gilon et al., 2000; Sadis et al., 1995). Despite hydrophobicity constituting a primary Doa10-recognition determinant (Hickey et al., 2021), not all QCAP degrons conform to the same consensus (Maurer et al., 2016). Overall, the initial degron discoveries, while gaining important insights into degron complexities, could not account for the entire QCAP.

A major barrier to unearthing QCAP degrons has been their unconformity. Therefore, authentic degron discovery largely relied on the screening of peptide libraries in search of sequences that induce the degradation of otherwise stable proteins and then, trying to deduce consensus sequence requirements (Fredrickson et al., 2011; Geffen et al., 2016; Gilon et al., 1998; Kats et al., 2018;

Koren et al., 2018; Lin et al., 2018; Maurer et al., 2016; Rosenbaum et al., 2011; Sadis et al., 1995). Indeed, these efforts led to the discovery of many artificial and physiological degrons but were still far from distinguishing common degradation motifs in QCAP. A breakthrough in degron discovery has been provided by the development of the pioneering GPS-peptidome methods to study protein degradation and identify degron motifs (Koren et al., 2018; Lin et al., 2018; Tokheim et al., 2021). By implementing GPS-P in yeast we have here identified a large cohort of authentic degrons that was subsequently used to train a degron prediction algorithm (Johansson et al., submitted). Thus, this large group of peptides that determine a variety of half-lives, provide consensus degron features that are compatible with TMD properties. Further functional validation established TM-like degron features as key determinants of QCAP and possibly of the proteome half-life.

That TMDs can operate as degrons is not surprising as membrane-embedded sequences within integral ER-membrane proteins have already been shown to display a degron function. These include the C-terminal TMD of the T-cell receptor α subunit (TCR α) (Bonifacino et al., 1990; Yu et al., 1997) as well as other lone proteins that are normally part of TM protein complexes (Habeck et al., 2015; Natarajan et al., 2020). Single and homomeric ER-embedded proteins, such as the E2 enzyme Ubc6 and the C-terminal TMDs of yeast and human HMG CoA reductase can similarly undergo QCAP via their TMDs that act as degrons (Gardner and Hampton, 1999; Ravid et al., 2000; Walter et al., 2001). By demonstrating that single-pass TM proteins devoid of their SPs were rapidly degraded by the UPS (Figures 4D, 4F), we have expanded this view by establishing TMDs as conserved QCAP degrons of non-integrated TM proteins.

Our findings that TMDs can act as degrons are compatible with a pre-insertion degradation mechanism, operating at the cytosolic side of the ER membrane, that subjects Signal Recognition

Particle (SRP)-independent substrates of the glycosylphosphatidylinositol (GPI) anchored proteins to QCAP (Ast et al., 2014). It is also compatible with SRP-independent insertion mechanisms of Atg27 and Ksh1 (Costa et al., 2018) that eliminate subpopulations that may evade the secretory pathway (Figure 4F). Moreover, in mammals, BAG6 and its associated protein UBQLN4 were shown to recognize the exposed hydrophobicity of TMDs of proteins that evade the secretory pathway and trigger their proteasomal degradation (Hessa et al., 2011; Suzuki and Kawahara, 2016). Thus, exposure of both the SP and TMDs may ensure that suboptimal or complete failure of ER membrane integration would result in QCAP. Failure to degrade mislocalized membrane proteins may result in cytotoxicity, due to enhanced formation of insoluble intracellular bodies or aberrant insertion in the mitochondria membrane (Costa et al., 2018). Our observation that SP-devoid integral membrane proteins are subjected to rapid degradation (Figures 4D-F) is fully compatible with this assumption.

The prevalence of QCAP degrons function was previously demonstrated by overlapping degron recognition by E3 ligases (Figure 5G and (Breckel and Hochstrasser, 2021)). As protein structure is dynamic, QCAP sensing of protein folding state via the exposure of TM-like domains and their nonselective E3 ligase recognition can now provide a plausible mechanism for regulation of the proteome stability. As E3 ligases are rate-limiting for ubiquitin-dependent degradation, recognition of common QCAP degron features by multiple E3 ligases may increase cellular degradation capacity in response to diverse stress conditions where aberrant protein overload might lead to proteotoxicity (Buchberger et al., 2010).

Molecular chaperones that discern misfolded proteins also participate in misfolded protein degradation (Kriegenburg et al., 2012; Shiber and Ravid, 2014). Auxiliary PQC chaperone functions include substrate solubilization, mediating E3 binding, as well as delivery of

ubiquitinated proteins to the proteasome (Shiber and Ravid, 2014). The prevailing mode of chaperones' function in QCAP asserts that Hsp70s initially recognize misfolded substrates and deliver them to an E3 ligase, a function facilitated by Hsp40s and nuclear exchange factors that catalyze ATP hydrolysis and ADP exchange, respectively (Abildgaard et al., 2020). While a role for Hsp70s/Hsp40s in misfolded substrate targeting to the human E3 ligase, carboxy-terminus of Hsc70 interacting protein (CHIP), is well established (McDonough and Patterson, 2003), whether Hsp70s/Hsp40s similarly mediate the recognition of QCAP degrons by their cognate E3s remains to be determined.

Conclusion

Adaptation of the GPS-P technology into yeast research facilitated the identification of QCAP degron sequences within the eukaryotic peptidome. The substantial number of identified degron sequences thus enabled a machine-learning algorithm to faithfully define consensus degron features. The ability of QCDPred to identify degrons in viral and human proteins (Figure 6), supports the notion that the majority of the proteome contains QCAP degrons with conserved characteristics.

The extent of TM-like degron function remains to be determined. Whether it is the "Holy Grail" that controls proteome stability or if other degron modules also play a substantial role remains to be elucidated. However, the properties of TM-like domains and their conditional exposure can now, for the first time, provide an expansive explanation to QCAP function in the maintenance of the eukaryotic proteome.

Acknowledgment

We are grateful to Prof. Richard Kulka for inspiration and support. We also thank Dr. Yuval Reiss for diligently reviewing the manuscript and Dr. Itay Koren for advice during the setup of

yGPS-P. B.M. acknowledges the support of the Neubauer doctoral fellowship fund. This work was supported by NSF-BSF grant 2016722 (to R.G.G and T.R) and the Novo Nordisk Foundation centre PRISM (NNF18OC0033950; to R.H.-P. and K.L.-L.).

Author contributions

Conceptualization, B.M., R.G.G. and T.R.; Methodology, B.M., R.G.G., T.R., K.E.J, K.L.L. R.H.P; Software, K.E.J., K.L.L., S.A., A.C., and N.F.; Validation, B.M.; Formal Analysis, K.E.J., and S.A.; Investigation, B.M., S.A., K.E.J., and T.R.; Resources, B.M., S.A.; Writing-Original Draft, B.M., S.A., and T.R.; and Writing-Review & Editing, K.E.J, K.L.L., R.H.P., R.G.G., N.F. and T.R.

Declaration of Interests

The authors declare no competing interests.

Figure titles and legends

Figure 1. Principles and validation of the yGPS-peptidome method.

(A) *Upper panel:* Schematic representation of yGPS-peptide library (yGPS-P_{lib}) where a peptide-DNA library comprised of 51mer tiled DNA fragments from 355 proteins, represented by different colors, are cloned in-frame downstream to GFP in the yGPS-P vector. The single mRNA product consists of yeCherry-IRES-yeGFP-peptide. *Lower panel*: DNA and protein sequences illustrating the cloning site that pursues GFP and the pentameric linker.

(B) Flowchart of the degron screen. yGPS-P_{lib} is transformed into yeast, followed by flow cytometry or FACS.

(C) *Upper panel*: Flow cytometry histograms of *CL1* or *DegAB* degrons appended to yGPS-P, in *wild type* and *doa10*Δ cells. Fluorescence emissions of 10,000 cells were determined for each

condition. *Lower panel*: Immunoblot analysis of the levels of *CL1*- and *DegAB*- appended GFP compared to Cherry loading control. yeG: yeGFP, yeC: yeCherry, EV: empty vector.

(D) Flow cytometry histogram of yeG/yeC in yGPS-P_{lib} compared to empty vector control.

(E) Proteasome dependence of GFP-appended peptides. Cells expressing yGPS-P_{lib} were treated with 10µM Bortezomib (BZ) for four hours or with DMSO vehicle control. Cells were subjected to immunoblotting with anti-ubiquitin Abs (left panel), or to flow cytometry analysis (middle panel). Shown in the right panel is the effect of BZ on a pre-selected degron library yGPS-P_{deg} composed of top10% degrons.

Figure 2. QCAP degrons functionality is largely defined by their amino acid composition.

(A) Fluorescence-activated cell sorting of yGPS-P_{lib} into four gates (G1-4), each composed of 2.5 million cells, was followed by NGS and protein stability index (PSI) scoring of each peptide. Shown is a FACS illustration and gating of 10,000 cells.

(B) Peptide density, based on their PSI values. Data were divided into six equal bins.

(C) Amino acid distribution within the six bins shown in B. *Left panel*: Heatmap of the overall distribution (in %) of amino acids in the different bins. *Right panel*: Fold change of amino acids distribution in the different bins compared to their average distribution in yGPS-P_{lib}.

(D) Flow cytometry histogram of peptide P3 with or without BZ.

(E) Flow cytometry histogram of intact or mutant P3 peptide in which three amino acids were replaced with either glutamate (E) or arginine (R) residues.

(F) 3D structure of QCDPred-calculated cytosolic Pca1 degron (amino acids 289-305), based on AlphaFold Pca1 structural model #AF-p38360-F1 (Conf. (90 > pLDDT > 70). Marked by a blue

color are the cysteine residues. Marked by a red color are the three amino acids that have been replaced with aspartate or arginine. pLDDT: per-residue confidence score in a scale of 0-100.

(G) Immunoblot analysis of Pca1 protein levels. *Wild type* or *doa10*Δ (*d*Δ) cells, expressing the indicated HA-tagged Pca1 proteins were left intact or treated with 50 μM $CdCl_2$ for 1 hour. To determine degradation dynamics, where indicated, the translation inhibitor cycloheximide (CHX) was added to cells for 15 min prior to cell harvesting. Pca1 levels were measured by immunoblotting using anti HA Abs while Pgk1 levels served as a loading control. D: replacement of residues marked in 2F by a red color with aspartate; R: replacement of residues marked in 2F by a red color with Arginine.

Figure 3. QCDPred assignment of TMDs as QCAP degrons.

(A) Map of degrons prediction by QCDPred (in grey) and TMDs prediction by TMHMM (in light blue) within Pca1 sequence. Marked by an arrowhead is the Pca1 cytosolic degron. A degron cutoff probability is marked at P = 0.85 by a dashed red line.

(B) Venn diagram of the relationship between yeast TMDs, extracted from the TM Helix Hidden Markov Model (TMHMM) algorithm, and QCDPred degron probabilities ($P \geq 0.85$).

(C) Assignment of QCDPred calculated degrons (in green) and TMHMM predicted TMDs (in yellow) to the cytochrome b-c1 complex (PDB #6T0B). overlay regions are colored in orange.

(D) Frequency distribution of (i) all QCDPred assigned degrons ($P \geq 0.85$), (ii) degrons composed of TMDs and (iii) degrons that are not part of a TMD, sorted into probability ranges between 0.85 -1.

Figure 4. Transmembrane domains function as QCAP degrons.

(A) Membrane localization of single-pass type-1 TM proteins, Erp2, Atg27, and Ksh1, determined by fluorescence microscopy.

(B) Map of QCDPred and TMHMM predictions of Erp2, Atg27, and Ksh1 degron and TMD probabilities, respectively. A degron cutoff probability is marked at P = 0.85 by a dashed red line.

(C, D, E, F). Flow cytometry histograms of the yeG/yeC ratio in cells expressing (C,D) C-terminal appended TMDs (C) or SPs (D), (E) N-terminal appended, full length and ΔSP proteins, and (F) C-terminal appended ΔSP proteins. Illustrated below each panel is the composition and domain order of the GFP appended proteins. TM: transmembrane, SP: signal peptide.

Figure 5. Characterization of QCAP degrons.

(A) Scatter plot comparing between Kyle-Doolittle hydrophobicity amino acid scores and QCDPred probabilities.

(B) Pie chart of the classification and relative proportions of protein secondary structure within the yeast proteome versus that of QCDPred-predicted degrons, based on the AlphaFold Protein Structure Database.

(C) Plot of the percentile of α helix structures versus QCDPred assigned non-TMD degron probabilities divided into four equal bins.

(D) Flow cytometry histograms of the yeG/yeC ratio in cells expressing P1 peptide emerged from the yeast protein COB and two randomly scrambled variants SC1 and SC2.

(E) Plot of QCDPred calculated degron centers, as a function of protein length. ρ: Spearman's correlation coefficient. $P_{value} < 0.0001$.

(F) Gene ontology (GO) process annotations of the fold change of top twelve significant pathways (P-value < 0.05) enriched or devoid of degrons, compared to a reference yeast proteome (strain S288C).

(G). Venn diagram displaying overlapping functions of the tested QCAP E3 enzymes. ΔPSI values between degrons in *pdr5*Δ strain (PSI < 1.7, 2175 peptides) *and E3*Δ strains were calculated. Sequences of top 10% ΔPSI values for each knockout strain (218 peptides) were compared.

Figure 6. Degron projections in non-yeast organisms

(A) *upper panel* Assignment of QCDPred projected degrons into the influenza C virus Polyprotein p42 trRosetta-predicted 3D structure (Template modeling score: 0.642). Shown is the schematics of p42 cleavage at an internal SP site (marked in purple) into p31 and CM2. *Lower panel*: QCDPred and TMHMM probabilities of p42 degrons (in grey) and TMDs (in light blue), respectively. *Arrowhead* indicates the position of the postulated p31 degron. `A degron cutoff probability is marked at P = 0.85 by a dashed red line.

(B) *Upper panel*: Assignment of a QCDPred-identified QCAP degron into the AlphFold-predicted SGK1 structure (#AF-O00141-F1). *Lower panel*: QCDPred-calculated degron probabilities within SGK1. *Arrowhead* indicates the position of the postulated SGK1 degron. A degron cutoff probability is marked at P = 0.85 by a dashed red line.

(C) Scatter plot comparing between PSI values of 23mer C-terminal peptides of the human proteome (Koren et al., 2018) and averaged QCDPred assessment of the same fragments. Prediction scores were averaged between 7 different amino acids centers within the 23 amino acids length of the original peptides. Shown are values of random 25% peptides from the Koren's screen. ρ: Spearman's correlation coefficient. $P_{value} < 0.0001$.

(D) Scatter plot comparing between PSI values of 15mer N-terminal peptides of the yeast *Saccharomyces cerevisiae* proteome (Kats et al., 2018) and QCDPred assessment of the same fragments. ρ: Spearman's correlation coefficient. $P_{value} < 0.0001$.

Materials and Methods

Parental plasmid for yGPS-P screen

Plasmid pGADT7-ADH700-yeCherry-p150-yeGFP-DHFR was obtained from Addgene (#24378) (Edwards and Wandless, 2010) and was used as a template for PCR cloning of ADH700-yeCherry-P150-yeGFP into pTR1412 (Geffen et al., 2016) at NotI and XmaI restriction sites. A 5-mer linker was added downstream to GFP to create the parental plasmid pTR1861 for yGPS-P screen (Figure 1A). pTR2089, the parental plasmid for yGPS-P N-terminal cloning, was constructed by overlap extension PCR (Hilgarth and Lanigan, 2020), producing a fragment containing PacI and BamHI restriction sites, that was placed upstream to GFP in pTR1861 by ligation.

Cloning and mutagenesis

Plasmids used in this study are listed below. DNA fragments encoding the full-length, ΔSP, TMD only and SP only versions of Erp2, Atg27, and Ksh1 were amplified from genomic DNA of *wild-type* yeast strain BY4741. The PCR fragments were subjected to digestion with restriction enzymes XmaI and NheI (for C-terminal cloning) or with PacI and BamHI (for N-terminal cloning). The resulting fragments were subcloned into pTR1861 or pTR2089, respectively.

Oligos insertions into pTR1861 were done by heating a single DNA pair containing the wanted insertion (see "Oligos Table" for details) and flanking sequences responsible for overhangs compatible with XmaI and NheI restriction sites and cooling down slowly to create double-

stranded fragments. The double-strand DNA was ligated directly into pTR1861, digested by the same restriction enzymes. Mutagenesis of peptide P3 and of Pca1 was conducted using QuikChange Lightning Site-Directed Mutagenesis Kit, according to the manufacturer's instructions (Agilent). All products were verified by sequencing.

Generation of a peptide library (yGPS-P_{lib})

Three hundred thirty-five proteins, corresponding to 23 yeast complexes were first encoded as DNA bases using the Saccharomyces Genome Database (SGD) website. Then, DNA corresponding to the open reading frame of each protein was divided into 51 bp (17-mer) fragments with 36 bp (12-mer) overlaps between neighboring oligonucleotides (tiling). The fragments also contained two flanking 12 bp primers that match the vector sequence to enable Gibson assembly. The corresponding oligonucleotides were synthesized by LC Sciences (Houston, TX), amplified by PCR, and cloned by Gibson assembly master mix kit (New England Biolabs) into pTR1861 at XmaI and NheI restriction sites, followed by transformation into electro-competent DH10B bacterial cells. Approximately two million colonies were scraped from plates and pooled and plasmid DNA was purified using PureLink® HiPure plasmid filter Midiprep kit (Invitrogen). The resulting plasmid library was transformed into TRy1392 *pdr5*Δ yeast strain, followed by selection on leucine-deficient media (SD-Leu). Surviving cells were scraped, pooled, and frozen immediately in 25% glycerol at -80°C.

Generation of a degron library (yGPS-P_{deg})

Yeast cells expressing yGPS-P_{lib} were grown O/N on SD-Leu media to mid-log phase. Cells were subjected to BD FACS Aria III instrument using 488 nm and 561 nm lasers for capturing the fluorescence emission of GFP and Cherry, respectively. One million cells having the lowest 10% yeG/yeC ratio, representing cells harboring unstable GFP, were separated (Supplemental Figure

1). Sorted cells were incubated O/N in SD-Leu media, then divided into aliquots and frozen in 25% glycerol at -80°C.

Degron screen

Cells expressing yGPS-P_{lib} were grown to mid-log-phase and sorted by FACS BD-Facsaria III into four equal gates, each contained 2.5 million yeast cells, based on their yeG/yeC ratio (Figure 2A). Plasmids from each gate were purified using Zymoprep yeast Plasmid Miniprep II (Zymo Research).

Preparation of plasmid DNA for NGS

DNA sequencing by NGS consisted of two PCR amplification steps with KAPA HiFi HotStart ReadyMix PCR Kit (Roche). The first step (18 cycles) was performed using primers flanking the peptides, with overhangs complementary to Illumina adapters (primers NGS-F, NGS-R). The second step was performed using standard N-series Illumina barcoded adapters (12 cycles). Sequences were size selected using SPRI beads for NGS. Samples were subsequently pooled, purified on an agarose gel, and sequenced on an Illumina NextSeq 500 machine.

Data pre-processing

Sequencing data were processed using a custom pipeline written for the R project for statistical computing (https://www.R-project.org). Reads were aligned to the expected oligo database with bowtie2 (Langmead and Salzberg, 2012). Sequences corresponding to the tiled peptides were counted and assigned to the different strains based on forward and reverse barcodes.

Protein stability indices (PSIs) were calculated according to Yen et al (Yen et al., 2008). Briefly, the frequency, f_{ig}, of peptide, i, in gate, g, was multiplied by gate number (1-4) and summed up, yielding a stability score between 1 (maximally unstable) and 4 (maximally unstable)

$$PSI_i = \frac{\sum_g g \times f_{ig}}{\sum_g f_{ig}}$$

Flow cytometry

Yeast cells were grown to mid-log-phase on SD-Leu media and analyzed on a CellStream analyzer instrument (Merck) using 488 nm and 561 nm lasers for capturing the fluorescence emission of GFP and Cherry, respectively. For each condition, 10,000 events were analyzed and presented on histogram using FlowJo software (BD Biosciences). Experiments were repeated two or more times.

Immunoblotting

Cells were grown to mid-log-phase and pelleted by centrifugation (3,500 × g, 5 min). Cells were incubated with 0.1N NaOH for 5 min, then pelleted by centrifugation (17,000 × g, 3 min) and SDS-PAGE sample buffer containing 50 mg/ml Dithiothreitol was added, followed by boiling for 5 min. Proteins were separated on SDS-PAGE, transferred to a PVDF membrane, blocked in 10% Dry Milk in TBS + 0.1% Tween-20 (TBS-T), and then probed with primary antibodies for one hour at room temperature. Following three washes with TBS-T, the membrane was incubated with a secondary antibody for 0.5 h at room temperature, then washed three times with TBS-T. Membranes were incubated with ECL mix (Thermo Fisher Scientific) for 2 min and reactive bands were visualized using Fusion Pulse (Vilber Lourmat).

Fluorescence Microscopy:

Imaging was performed with Olympus IX71 inverted microscope with an x 60 oil objective lens. Fluorescence was excited with 576 nm for Cherry and with 488 nm for GFP. Imaging data were handled using ImageJ.

Proteome Databases

All proteome databases were downloaded from the UniProt database server (https://www.uniprot.org) as FASTA files. These files contain the full-length protein sequence.

PDB/CIF data

AlphaFold-2 based PDB and CIF files for single proteins were extracted from the European Bioinformatics Institute website (https://alphafold.ebi.ac.uk/). These files were used for creating a 3D proteins database. Most PDB and CIF files contain information on secondary structure patterns. Each amino acid in these models was assigned secondary structure indicator and proteome statistics were inferred.

Transmembrane protein Data

Transmembrane protein data was extracted from the TM Helix Hidden Markov Model (TMHMM) algorithm (Krogh et al., 2001; Tusnády and Simon, 1998), implemented with python package tmhmm.py. To compute the intersection between TMDs and degrons, each amino acid within the entire yeast proteome was evaluated for QCDPred value and TMD classification. Amino acids with QCDPred probability ≥ 0.85 that were classified as TMDs according to TMHMM were added to the intersection group.

Antibodies used in this study:

Polyclonal Rabbit anti-GFP	Abcam	ab290
Monoclonal Rabbit anti-mCherry	Abcam	ab213511
Monoclonal Rat anti-HA	Roche	11867423001
Monoclonal Mouse anti-PGK1	Abcam	ab113687
Polyclonal Rabbit anti-G6PD	Sigma Israel	a9521
Polyclonal Rabbit anti-Ubiquitin	Dako	Z0458
Goat anti-Rabbit	ImmunoResearch	111035144
Goat anti-Mouse	ImmunoResearch	115035062
Goat anti-Rat	ImmunoResearch	112035062

Chemicals:

Chemical	Manufacturer	Catalog #
Bortezomib (BZ)	A2S	A2614
Cadmium	Sigma	265365

Yeast strains used in this study:

Strain name	Genotype
BY4741	*MATa met15Δ0, ura3Δ0, leu2Δ0, his3Δ1*
TRy1121	*MATa met15Δ0, ura3Δ0, leu2Δ0, his3Δ1, doa10::KanMX*
TRy1373	*MATa met15Δ0, ura3Δ0, leu2Δ0, his3Δ1, ubr1::KanMX*
TRy1388	*MATa met15Δ0, ura3Δ0, leu2Δ0, his3Δ1, san1::KanMX*
TRy1392	*MATa met15Δ0, ura3Δ0, leu2Δ0, his3Δ1, pdr5::KanMX*

Oligos Table:

Name	Sequence
NGS-F	TCGTCGGCAGCGTCAGATGTGTATAAGAGACANNNGGATCAGCTGGCTCACCC
NGS-R	GTCTCGTGGGCTCGGAGATGTGTATAAGAGACAGANNNACATAACTAATTACATGATCAGTCAGCT
P3-F	CCGGGTTCAAACGAAACGCTGTTTTTGTTGGTACTATCTTTGCAGGTGCCTTTGTTTGAG
P3 E_{mut}- F	CCGGGTTCAAACGAAACGCTGTTTTTGTTGGTACTGAGGAGGCAGGTGCCGAGGTTTGAG
P3 E_{mut} -R	CTAGCTCAAACCTCGGCACCTGCCTCCTCAGTACCAACAAAAACAGCGTTTCGTTTGAAC
P3 R_{mut}- F	CCGGGTTCAAACGAAACGCTGTTTTTGTTGGTACTCGTCGTGCAGGTGCCCGTGTTTGAG
P3 R_{mut}- R	CTAGCTCAAACACGGGCACCTGCACGACGAGTACCAACAAAAACAGCGTTTCGTTTGAAC
P3-R	CTAGCTCAAACAAAGGCACCTGCAAAGATAGTACCAACAAAAACAGCGTTTCGTTTGAAC
P1-F	CCGGGTATTTAGTACCTTTTATCATTGCTGCAATGGTTATTATGCATTTAATGGCATGAG
P1-R	CTAGCTCATGCCATTAAATGCATAATAACCATTGCAGCAATGATAAAAGGTACTAAATAC
SC1-F	CCGGGATCTTATTTATGGTAGCTATTCCTGTTCATGCAATTGCATATTTAATGATGTGAG
SC1-R	CTAGCTCACATCATTAAATATGCAATTGCATGAACAGGAATAGCTACCATAAATAAGATC
SC2-F	CCGGGCATGCTGCAATCATGTATATGGCAGTTATTGTATTAATTTTTTTAATGCCTTGAG
SC2-R	CTAGCTCAAGGCATTAAAAAAATTAATACAATAACTGCCATATACATGATTGCAGCATGC

List of plasmids used in this study

Unless indicated otherwise, clones are C-terminal fusions to yeGFP

	Description	Additional information
pTR1494	pRS416-GPDp-HA-Pca1	adle et al. PNAS 2009
pTR1859	pRS315-ADH700p-yeCherry-p150-yeGFP-XmaI,NheI-CYCt	
pTR1861	pRS315-ADH700p-yeCherry-p150-yeGFP-linker-XmaI,NheI-CYCt	Vector for C-terminal fusion to yeG
pTR1882	pRS315-ADH700p-yeCherry-p150-yeGFP-linker-XmaI-*CL1*-NheI-CYCt	
pTR1884	pRS315-ADH700p-yeCherry-p150-yeGFP-linker-XmaI-*DegAB*-NheI-CYCt	
pTR2036	pRS315-ADH700p-yeCherry-p150-yeGFP-linker-XmaI-P1-NheI-CYCt	
pTR2038	pRS315-ADH700p-yeCherry-p150-yeGFP-linker-XmaI-P3-NheI-CYCt	
pTR2058	pRS315-ADH700p-yeCherry-p150-yeGFP-linker-XmaI-P3$_{EE}$-NheI-CYCt	Replacing TIFAGAFV with TEEAGAEV
pTR2060	pRS315-ADH700p-yeCherry-p150-yeGFP-linker-XmaI-P3$_{RR}$-NheI-CYCt	Replacing TIFAGAFV with TRRAGARV
pTR2089	pRS315-ADH700p-yeCherry-p150-PacI,BamHI-yeGFP-linker-XmaI,NheI-CYCt	Vector for N-terminal fusion to yeG
pTR2124	pRS416-GPDp-HA-Pca1$_{DD}$	Replacing LGCICNY with LDCDCDY
pTR2127	pRS315-ADH700p-yeCherry-p150-yeGFP-linker-XmaI-$_{\Delta sp}$Erp2-NheI-CYCt	
pTR2128	pRS315-ADH700p-yeCherry-p150-yeGFP-linker-XmaI-$_{\Delta sp}$Atg27-NheI-CYCt	
pTR2129	pRS315-ADH700p-yeCherry-p150-yeGFP-linker-XmaI-$_{\Delta sp}$Ksh1-NheI-CYCt	
pTR2149	pRS315-ADH700p-yeCherry-p150-PacI-Erp2-BamHI-yeGFP-linker-CYCt	N-terminal fusion
pTR2151	pRS315-ADH700p-yeCherry-p150-PacI-Atg27-BamHI-yeGFP-linker-CYCt	N-terminal fusion
pTR2152	pRS315-ADH700p-yeCherry-p150-PacI-Ksh1-BamHI-yeGFP-linker-CYCt	N-terminal fusion
pTR2153	pRS315-ADH700p-yeCherry-p150-PacI-$_{\Delta sp}$Erp2-BamHI-yeGFP-linker-CYCt	N-terminal fusion
pTR2155	pRS315-ADH700p-yeCherry-p150-PacI-$_{\Delta sp}$Atg27-BamHI-yeGFP-linker-CYCt	N-terminal fusion
pTR2156	pRS315-ADH700p-yeCherry-p150-PacI-$_{\Delta sp}$Ksh1-BamHI-yeGFP-linker-CYCt	N-terminal fusion
pTR2160	pRS315-ADH700p-yeCherry-p150-yeGFP-linker-XmaI-SP(Ksh1)-NheI-CYCt	SP of Ksh1 (aa 1-26)
pTR2162	pRS315-ADH700-yeCherry-p150-yeGFP-linker-XmaI-SP(Erp2)-NheI-CYCt	SP of Erp2 (aa 1-26)
pTR2164	pRS315-ADH700p-yeCherry-p150-yeGFP-linker-XmaI-SP(Atg27)-NheI-CYCt	SP of Atg27 (aa 1-19)
pTR2167	pRS416 GPD HA-Pca1$_{RR}$	replacing LGCICNY with LRCRCRY
pTR2171	pRS315-ADH700p-yeCherry-p150-yeGFP-linker-XmaI-SC1-NheI-CYCt	Scrambled P1, variant #1
pTR2172	pRS315-ADH700p-yeCherry-p150-yeGFP-linker-XmaI-SC2-NheI-CYCt	Scrambled P1, variant #2
pTR2213	pRS315-ADH700p-yeCherry-p150-yeGFP-linker-XmaI-TMD(Atg27)-NheI-CYCt	TMD of Atg27 (aa 200-220)
pTR2214	pRS315-ADH700p-yeCherry-p150-yeGFP-linker-XmaI-TMD(Erp2)-NheI-CYCt	TMD of Erp2 (aa 183-203)
pTR2215	pRS315-ADH700p-yeCherry-p150-yeGFP-linker-XmaI-TMD(Ksh1)-NheI-CYCt	TMD of Ksh1 (aa 54-72)

Supplemental Information titles and legends

Supplemental Figures

Supplemental Figure 1, related to Figure 1. Isolation of top 10% degrons. Yeast cells expressing yGPS-P_{lib} Were grown to mid-log-phase, followed by FACS of top 10% degron population. One million cells comprising the degron library (yGPS-P_{deg}) were collected, then grown O/N and frozen in liquid nitrogen or taken for further analysis. Illustrated is gating of top 10% degron population out of a total of 10,000 cells.

Supplemental Figure 2. related to Figure 2. Maps of PSI values emerged from experimental data (black dots), average PSI values for each amino acid (colored in black) and calculated QCDPred probabilities (colored in red) were plotted for each of the proteins in the screen that reach 100% coverage (N=306).

Supplemental Figure 3, related to figure 3. Degrons in the b-c1 complex. (A) PSI values emerged from experimental data (black dots), average PSI values for each amino acid (colored in black), QCDPred probabilities (colored in red), and TMHMM prediction (colored in light blue) were plotted for each subunit of the b-c1 complex. A degron cutoff probability is marked at P = 0.85 by a dashed grey line. (B) Assignment of QCDPred projected Degrons (green) and TMHMM predicted TMDs (yellow) to TM proteins in the b-c1 3D structure (PDB #6t0b). Overlying regions are colored in orange.

Supplemental Figure 4, related to Figure 4. Immunoblot analysis of Erp2, Atg27 and Ksh1, with or without their SPs. Where indicated, 10 µM of Bortezomib (BZ) were added to cells for 4 hrs prior to cell harvesting. *FL*- full length proteins. Δ*SP*- proteins devoid of the SP.

Supplemental Figure 5, Related to Figure 5. Comparison of mean amino acid distribution within TMDs with high degron probability ($P \geq 0.85$, N=6,064) to those with lower probability ($P < 0.85$, N=107). Error bars represent low and high confidence intervals.

Supplemental Figure 6, related to Figure 5. Structure prediction of GFP-fused peptides using trRosseta. Estimated Template Modeling scores: COB- 0.856, SC1-0.865, SC2-0.828.

Supplemental Figure 7, related to Figure 5. Large-scale GO annotations of all significant processes (p-value < 0.05) that are either enriched or devoid of predicted degrons at $P \geq 0.85$.

Supplemental Figure 8, related to figure 5. QCDPred analysis of key cytosolic/nuclear yeast chaperones. A degron cutoff probability is marked at P = 0.85 by a dashed red line.

Supplemental Tables

Supplemental Table 1, related to Figure 1. proteins in the screen and the complex they belong to.

Supplemental Table 2, related to Figure 2. List of peptides in the screen and their PSI scores.

Supplemental Table 3, related to Figure 2. QCDPred analysis of proteins in the screen that reach 100% coverage (N = 306)

Supplemental Table 4, related to Figure 6. QCDPred analysis of the yeast proteome.

Supplemental Table 5, related to Figure 6. QCDPred analysis of the human proteome.

References

Abildgaard, A.B., Gersing, S.K., Larsen-Ledet, S., Nielsen, S. V, Stein, A., Lindorff-Larsen, K., and Hartmann-Petersen, R. (2020). Co-Chaperones in Targeting and Delivery of Misfolded Proteins to the 26S Proteasome. Biomolecules *10*.

Adle, D.J., and Lee, J. (2008). Expressional control of a cadmium-transporting P1B-type ATPase by a metal sensing degradation signal. J. Biol. Chem. *283*, 31460–31468.

Alfassy, O.S.O.S., Cohen, I., Reiss, Y., Tirosh, B., and Ravid, T. (2013). Placing a disrupted degradation motif at the C terminus of proteasome substrates attenuates degradation without impairing ubiquitylation. J. Biol. Chem. *288*, 12645–12653.

Amm, I., Sommer, T., and Wolf, D.H. (2014). Protein quality control and elimination of protein waste: The role of the ubiquitin–proteasome system. Biochim Biophys Acta *1843*, 182–196.

Ang, X.L., and Wade Harper, J. (2005). SCF-mediated protein degradation and cell cycle control. Oncogene *24*, 2860–2870.

Arteaga, M.F.M.F., Wang, L., Ravid, T., Hochstrasser, M., and Canessa, C.M.C.M. (2006). An amphipathic helix targets serum and glucocorticoid-induced kinase 1 to the endoplasmic reticulum-associated ubiquitin-conjugation machinery. Proc. Natl. Acad. Sci. *103*, 11178–11183.

Ast, T., Aviram, N., Chuartzman, S.G., and Schuldiner, M. (2014). A cytosolic degradation pathway, prERAD, monitors pre-inserted secretory pathway proteins. J. Cell Sci. *127*, 3017–3023.

Balchin, D., Hayer-Hartl, M., and Hartl, F.U. (2016). In vivo aspects of protein folding and quality control. Science *353*, aac4354.

Bonifacino, J.S., Suzuki, C.K., and Klausner, R.D. (1990). A peptide sequence confers retention and rapid degradation in the endoplasmic reticulum. Science *247*, 79–82.

Breckel, C.A., and Hochstrasser, M. (2021). Ubiquitin Ligase Redundancy and Nuclear-Cytoplasmic Localization in Yeast Protein Quality Control. Biomol. *11*.

Buchberger, A., Bukau, B., and Sommer, T. (2010). Protein Quality Control in the Cytosol and the Endoplasmic Reticulum: Brothers in Arms. Mol. Cell *40*, 238–252.

Christiano, R., Nagaraj, N., Fröhlich, F., and Walther, T.C. (2014). Global proteome turnover analyses of the Yeasts S. cerevisiae and S. pombe. Cell Rep. *9*, 1959–1965.

Costa, E.A., Subramanian, K., Nunnari, J., and Weissman, J.S. (2018). Defining the physiological role of SRP in protein-targeting efficiency and specificity. Science *359*, 689–692.

Davey, N.E., and Morgan, D.O. (2016). Building a Regulatory Network with Short Linear Sequence Motifs: Lessons from the Degrons of the Anaphase-Promoting Complex. Mol. Cell *64*, 12–23.

Deng, M., and Hochstrasser, M. (2006). Spatially regulated ubiquitin ligation by an ER/nuclear membrane ligase. Nature *443*, 827–831.

Eden, E., Geva-Zatorsky, N., Issaeva, I., Cohen, A., Dekel, E., Danon, T., Cohen, L., Mayo, A., and Alon, U. (2011). Proteome half-life dynamics in living human cells. Science *331*, 764–768.

Edwards, S.R., and Wandless, T.J. (2010). Dicistronic regulation of fluorescent proteins in the budding yeast Saccharomyces cerevisiae. Yeast *27*, 229–236.

Ella, H., Reiss, Y., and Ravid, T. (2019). The Hunt for Degrons of the 26S Proteasome. Biomolecules *9*.

Filipčík, P., Curry, J.R., and Mace, P.D. (2017). When Worlds Collide-Mechanisms at the Interface between Phosphorylation and Ubiquitination. J. Mol. Biol. *429*, 1097–1113.

Fredrickson, E.K., Rosenbaum, J.C., Locke, M.N., Milac, T.I., and Gardner, R.G. (2011). Exposed hydrophobicity is a key determinant of nuclear quality control degradation. Mol Biol Cell *22*, 2384–2395.

Furth, N., Gertman, O.O., Shiber, A., Alfassy, O.S.O.S., Cohen, I., Rosenberg, M.M.M.M., Doron, N.K.N.K., Friedler, A., and Ravid, T. (2011). Exposure of bipartite hydrophobic signal triggers nuclear quality control of Ndc10 at the endoplasmic reticulum/nuclear envelope. Mol.

Biol. Cell *22*, 4726–4739.

Gardner, R.G., and Hampton, R.Y. (1999). A “distributed degron” allows regulated entry into the ER degradation pathway. Embo J *18*, 5994–6004.

Gardner, R.G., Nelson, Z.W., and Gottschling, D.E. (2005). Degradation-mediated protein quality control in the nucleus. Cell *120*, 803–815.

Geffen, Y., Appleboim, A., Gardner, R.G.R.G., Friedman, N., Sadeh, R., and Ravid, T. (2016). Mapping the landscape of a eukaryotic degronome. Mol. Cell *63*, 1055–1065.

Gilon, T., Chomsky, O., and Kulka, R.G. (1998). Degradation signals for ubiquitin system proteolysis in Saccharomyces cerevisiae. Embo J *17*, 2759–2766.

Gilon, T., Chomsky, O., and Kulka, R.G. (2000). Degradation signals recognized by the Ubc6p-Ubc7p ubiquitin-conjugating enzyme pair. Mol Cell Biol *20*, 7214-9.

Guharoy, M., Bhowmick, P., Sallam, M., and Tompa, P. (2016). Tripartite degrons confer diversity and specificity on regulated protein degradation in the ubiquitin-proteasome system. Nat Commun *7*, 10239.

Habeck, G., Ebner, F.A., Shimada-Kreft, H., and Kreft, S.G. (2015). The yeast ERAD-C ubiquitin ligase Doa10 recognizes an intramembrane degron. J Cell Biol *209*, 261–273.

Hegde, R.S., and Keenan, R.J. (2022). The mechanisms of integral membrane protein biogenesis. Nat. Rev. Mol. Cell Biol. *23*, 107–124.

Hershko, A., Heller, H., Eytan, E., and Reiss, Y. (1986). The protein substrate binding site of the ubiquitin-protein ligase system. J Biol Chem *261*, 11992-9.

Hessa, T., Sharma, A., Mariappan, M., Eshleman, H.D., Gutierrez, E., and Hegde, R.S. (2011). Protein targeting and degradation are coupled for elimination of mislocalized proteins. Nature *475*, 394–397.

Hickey, C.M., Breckel, C., Zhang, M., Theune, W.C., and Hochstrasser, M. (2021). Protein quality control degron-containing substrates are differentially targeted in the cytoplasm and nucleus by ubiquitin ligases. Genetics *217*, 1–19.

Hilgarth, R.S., and Lanigan, T.M. (2020). Optimization of overlap extension PCR for efficient transgene construction. MethodsX *7*, 100759.

Hochstrasser, M., and Varshavsky, A. (1990). In vivo degradation of a transcriptional regulator: the yeast a2 repressor. Cell *61*, 697–708.

Johnson, P.R., Swanson, R., Rakhilina, L., and Hochstrasser, M. (1998). Degradation signal masking by heterodimerization of MATa2 and MATa1 blocks their mutual destruction by the ubiquitin-proteasome pathway. Cell *94*, 217–227.

Jumper, J., Evans, R., Pritzel, A., Green, T., Figurnov, M., Ronneberger, O., Tunyasuvunakool, K., Bates, R., Žídek, A., Potapenko, A., et al. (2021). Highly accurate protein structure prediction with AlphaFold. Nature *596*, 583–589.

Kästle, M., and Grune, T. (2012). Interactions of the proteasomal system with chaperones: protein triage and protein quality control. Prog. Mol. Biol. Transl. Sci. *109*, 113–160.

Kats, I., Khmelinskii, A., Kschonsak, M., Huber, F., Kniess, R.A., Bartosik, A., and Knop, M. (2018). Mapping Degradation Signals and Pathways in a Eukaryotic N-terminome. Mol Cell *70*, 488-501 e5.

Kim, Y.E., Hipp, M.S., Bracher, A., Hayer-Hartl, M., Ulrich Hartl, F., and Hartl, F.U. (2013). Molecular chaperone functions in protein folding and proteostasis. Annu. Rev. Biochem. *82*, 323–355.

Koliopoulos, M.G., and Alfieri, C. (2021). Cell cycle regulation by complex nanomachines. FEBS J.

Koren, I., Timms, R.T., Kula, T., Xu, Q., Li, M.Z., and Elledge, S.J. (2018). The Eukaryotic Proteome Is Shaped by E3 Ubiquitin Ligases Targeting C-Terminal Degrons. Cell *173*, 1622-1635 e14.

Kriegenburg, F., Ellgaard, L., and Hartmann-Petersen, R. (2012). Molecular chaperones in targeting misfolded proteins for ubiquitin-dependent degradation. FEBS J *279*, 532–542.

Krogh, A., Larsson, B., von Heijne, G., and Sonnhammer, E.L. (2001). Predicting transmembrane protein topology with a hidden Markov model: application to complete genomes. J Mol Biol *305*, 567–580.

Langmead, B., and Salzberg, S.L. (2012). Fast gapped-read alignment with Bowtie 2. Nat. Methods *9*, 357–359.

Leppert, G., McDevitt, R., Falco, S.C., Van Dyk, T.K., Ficke, M.B., and Golin, J. (1990). Cloning by gene amplification of two loci conferring multiple drug resistance in Saccharomyces. Genetics *125*, 13–20.

Lin, H.C., Yeh, C.W., Chen, Y.F., Lee, T.T., Hsieh, P.Y., Rusnac, D. V, Lin, S.Y., Elledge, S.J., Zheng, N., and Yen, H.S. (2018). C-Terminal End-Directed Protein Elimination by CRL2 Ubiquitin Ligases. Mol Cell *70*, 602-613 e3.

Lucas, X., and Ciulli, A. (2017). Recognition of substrate degrons by E3 ubiquitin ligases and modulation by small-molecule mimicry strategies. Curr. Opin. Struct. Biol. *44*, 101–110.

Marzioch, M., Henthorn, D.C., Herrmann, J.M., Wilson, R., Thomas, D.Y., Bergeron, J.J., Solari, R.C., and Rowley, A. (1999). Erp1p and Erp2p, partners for Emp24p and Erv25p in a yeast p24 complex. Mol. Biol. Cell *10*, 1923–1938.

Maurer, M.J., Spear, E.D., Allen, T.Y., Lee, E.J., Shahzad, S., and Michaelis, S. (2016). Degradation signals for ubiquitin-proteasome dependent cytosolic protein quality control

(CytoQC) in yeast. G3 Genes, Genomes, Genet. g3. 116.027953.

McCracken, A.A., and Brodsky, J.L. (1996). Assembly of ER-associated protein degradation in vitro: dependence on cytosol, calnexin, and ATP. J. Cell Biol. *132*, 291–298.

McDonough, H., and Patterson, C. (2003). CHIP: a link between the chaperone and proteasome systems. Cell Stress Chaperones *8*, 303–308.

Mészáros, B., Kumar, M., Gibson, T.J., Uyar, B., and Dosztányi, Z. (2017). Degrons in cancer. Sci. Signal. *10*.

Natarajan, N., Foresti, O., Wendrich, K., Stein, A., and Carvalho, P. (2020). Quality Control of Protein Complex Assembly by a Transmembrane Recognition Factor. Mol. Cell *77*, 108-119.e9.

Padovani, C., Jevtić, P., and Rapé, M. (2022). Quality control of protein complex composition. Mol. Cell.

Pekosz, A., and Lamb, R.A. (2000). Identification of a membrane targeting and degradation signal in the p42 protein of influenza C virus. J. Virol. *74*, 10480–10488.

Prasad, R., Xu, C., and Ng, D.T.W. (2018). Hsp40/70/110 chaperones adapt nuclear protein quality control to serve cytosolic clients. J. Cell Biol. *217*, 2019–2032.

Rape, M. (2018). Ubiquitylation at the crossroads of development and disease. Nat. Rev. Mol. Cell Biol. *19*, 59–70.

Ravid, T., Doolman, R., Avner, R., Harats, D., and Roitelman, J. (2000). The ubiquitin-proteasome pathway mediates the regulated degradation of mammalian 3-hydroxy-3-methylglutaryl-coenzyme A reductase. J. Biol. Chem. *275*, 35840–35847.

Rosenbaum, J.C., Fredrickson, E.K., Oeser, M.L., Garrett-Engele, C.M., Locke, M.N., Richardson, L.A., Nelson, Z.W., Hetrick, E.D., Milac, T.I., Gottschling, D.E., et al. (2011). Disorder Targets Misorder in Nuclear Quality Control Degradation: A Disordered Ubiquitin

Ligase Directly Recognizes Its Misfolded Substrates. Mol. Cell *41*, 93–106.

Sadis, S., Atienza Jr., C., and Finley, D. (1995). Synthetic signals for ubiquitin-dependent proteolysis. Mol Cell Biol *15*, 4086–4094.

Samant, R.S., Livingston, C.M., Sontag, E.M., and Frydman, J. (2018). Distinct proteostasis circuits cooperate in nuclear and cytoplasmic protein quality control. Nature *563*, 407.

Shiber, A., and Ravid, T. (2014). Chaperoning proteins for destruction: diverse roles of Hsp70 chaperones and their co-chaperones in targeting misfolded proteins to the proteasome. Biomolecules *4*, 704–724.

Smith, N., Wei, W., Zhao, M., Qin, X., Seravalli, J., Kim, H., and Lee, J. (2016). Cadmium and Secondary Structure-dependent Function of a Degron in the Pca1p Cadmium Exporter. J Biol Chem *291*, 12420–12431.

Sontag, E.M., Samant, R.S., and Frydman, J. (2017). Mechanisms and Functions of Spatial Protein Quality Control. Annu. Rev. Biochem. *86*, 97–122.

Suzuki, R., and Kawahara, H. (2016). UBQLN4 recognizes mislocalized transmembrane domain proteins and targets these to proteasomal degradation. EMBO Rep. *17*, 842–857.

Swanson, R., Locher, M., and Hochstrasser, M. (2001). A conserved ubiquitin ligase of the nuclear envelope/endoplasmic reticulum that functions in both ER-associated and Matalpha2 repressor degradation. Genes Dev *15*, 2660-74.

Tokheim, C., Wang, X., Timms, R.T., Zhang, B., Mena, E.L., Wang, B., Chen, C., Ge, J., Chu, J., Zhang, W., et al. (2021). Systematic characterization of mutations altering protein degradation in human cancers. Mol. Cell *81*, 1292-1308.e11.

Trumpower, B.L. (1990). Cytochrome bc1 complexes of microorganisms. Microbiol. Rev. *54*, 101–129.

Tusnády, G.E., and Simon, I. (1998). Principles governing amino acid composition of integral membrane proteins: application to topology prediction. J. Mol. Biol. *283*, 489–506.

Tyedmers, J., Mogk, A., and Bukau, B. (2010). Cellular strategies for controlling protein aggregation. Nat Rev Mol Cell Biol *11*, 777–788.

Varadi, M., Anyango, S., Deshpande, M., Nair, S., Natassia, C., Yordanova, G., Yuan, D., Stroe, O., Wood, G., Laydon, A., et al. (2022). AlphaFold Protein Structure Database: massively expanding the structural coverage of protein-sequence space with high-accuracy models. Nucleic Acids Res. *50*, D439–D444.

Varshavsky, A. (1991). Naming a targeting signal. Cell *64*, 13–15.

Walter, J., Urban, J., Volkwein, C., and Sommer, T. (2001). Sec61p-independent degradation of the tail-anchored ER membrane protein Ubc6p. Embo J *20*, 3124-31.

Wendler, F., Gillingham, A.K., Sinka, R., Rosa-Ferreira, C., Gordon, D.E., Franch-Marro, X., Peden, A.A., Vincent, J.-P., and Munro, S. (2010). A genome-wide RNA interference screen identifies two novel components of the metazoan secretory pathway. EMBO J. *29*, 304–314.

Yen, H.-C.C.S., Xu, Q., Chou, D.M., Zhao, Z., and Elledge, S.J. (2008). Global protein stability profiling in mammalian cells. Science (80-.). *322*, 918–923.

Yen, W.-L., Legakis, J.E., Nair, U., and Klionsky, D.J. (2007). Atg27 is required for autophagy-dependent cycling of Atg9. Mol. Biol. Cell *18*, 581–593.

Yu, H., Kaung, G., Kobayashi, S., and Kopito, R.R. (1997). Cytosolic degradation of T-cell receptor alpha chains by the proteasome. J. Biol. Chem. *272*, 20800–20804.

Zheng, N., and Shabek, N. (2017). Ubiquitin Ligases: Structure, Function, and Regulation. Annu. Rev. Biochem. *86*, 129–157.

Figure 1

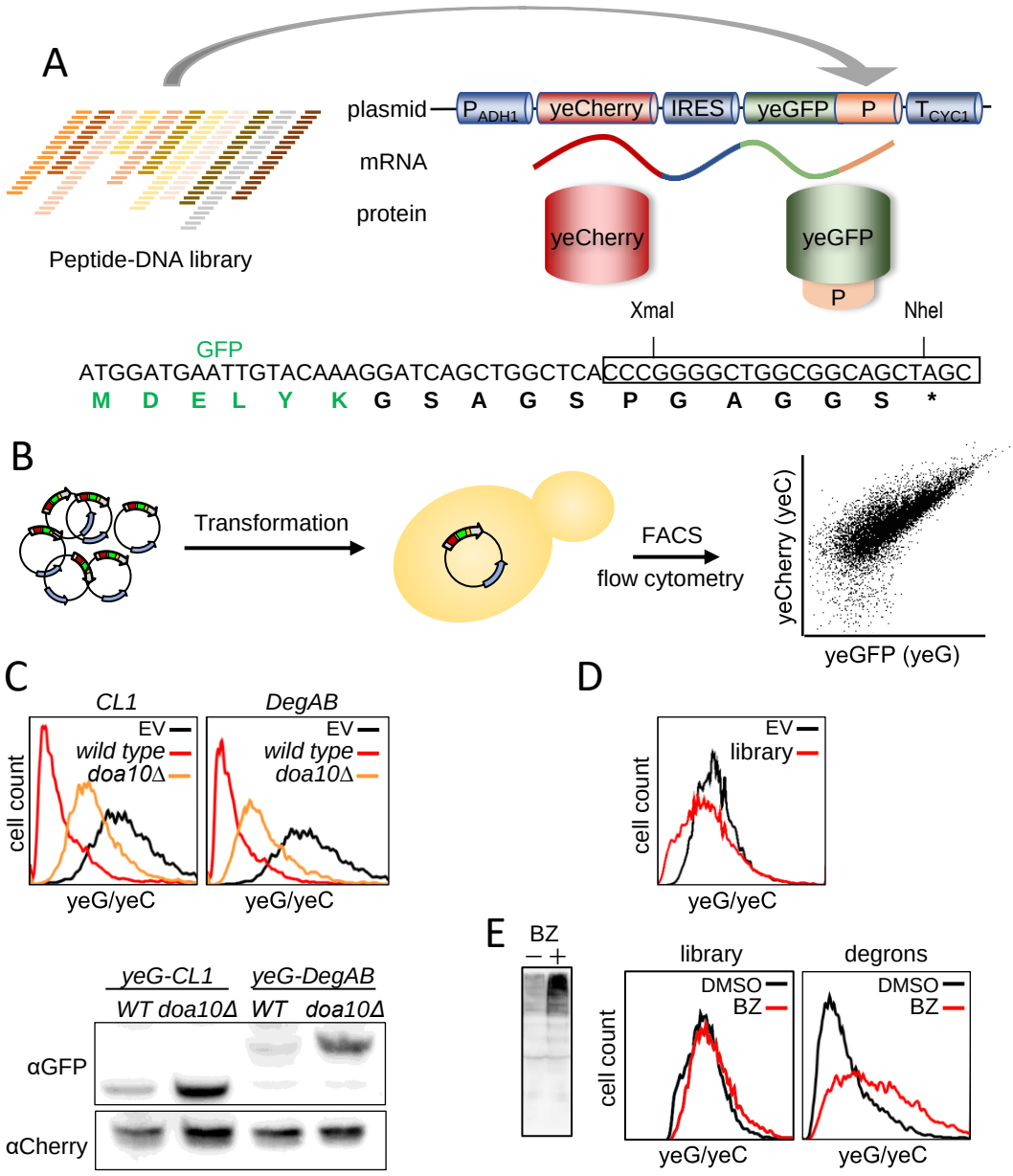
A
Peptide-DNA library
plasmid
P_{ADH1}
yeCherry
IRES
yeGFP
P
T_{CYC1}
mRNA
protein
yeCherry
yeGFP
P
XmaI
NheI
GFP
ATGGATGAATTGTACAAAGGATCAGCTGGCTCACCCGGGGCTGGCGGCAGCTAGC
M D E L Y K G S A G S P G A G G S *
B
Transformation
FACS
flow cytometry
yeCherry (yeC)
yeGFP (yeG)
C
CL1
DegAB
EV
wild type
doa10Δ
cell count
yeG/yeC
yeG-CL1
yeG-DegAB
WT doa10Δ WT doa10Δ
αGFP
αCherry
D
EV
library
cell count
yeG/yeC
E
BZ
− +
library
degrons
DMSO
BZ
cell count
yeG/yeC

Figure 2

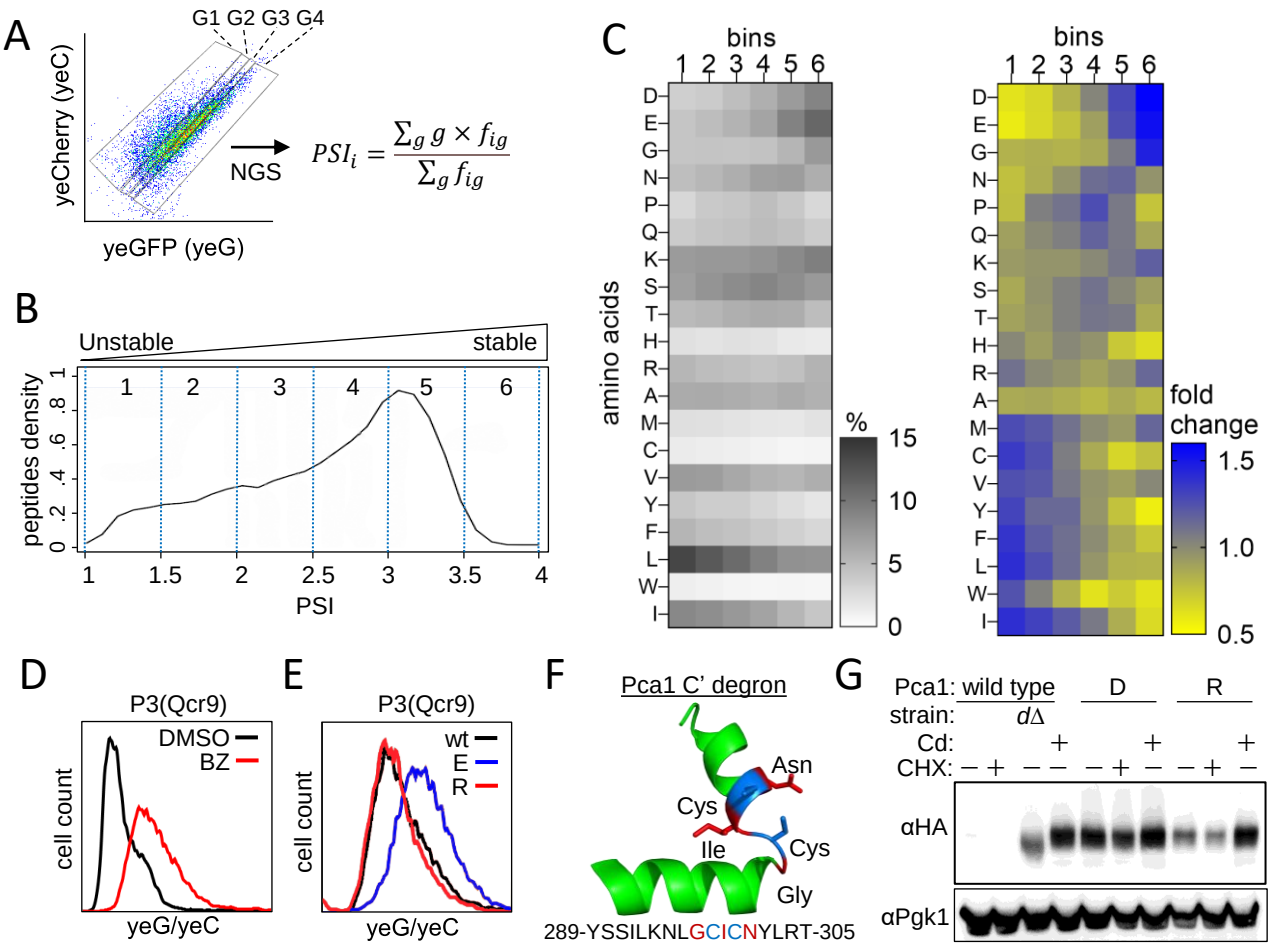
A
G1 G2 G3 G4
yeCherry (yeC)
yeGFP (yeG)
NGS
$PSI_i = \frac{\sum_g g \times f_{ig}}{\sum_g f_{ig}}$
B
Unstable
stable
peptides density
1 2 3 4 5 6
PSI
C
bins
amino acids
D E G N P Q K S T H R A M C V Y F L W I
%
fold change
D
P3(Qcr9)
DMSO
BZ
cell count
yeG/yeC
E
P3(Qcr9)
wt
E
R
cell count
yeG/yeC
F
Pca1 C' degron
Asn
Cys
Ile
Cys
Gly
289-YSSILKNLGCICNYLRT-305
G
Pca1: wild type D R
strain: dΔ
Cd:
CHX:
αHA
αPgk1

Figure 3

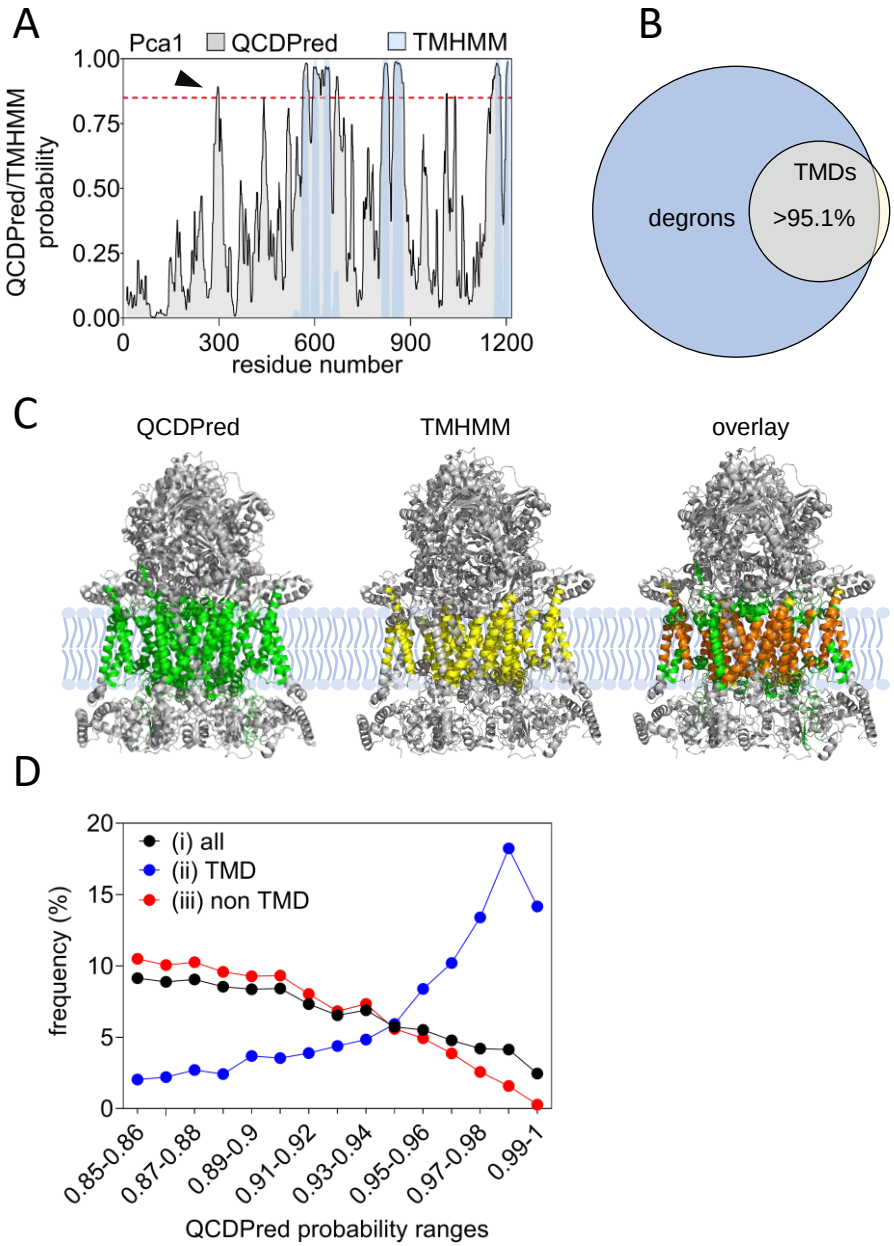
A
Pca1
QCDPred
TMHMM
QCDPred/TMHMM probability
1.00
0.75
0.50
0.25
0.00
0
300
600
900
1200
residue number
B
degrons
TMDs
>95.1%
C
QCDPred
TMHMM
overlay
D
(i) all
(ii) TMD
(iii) non TMD
frequency (%)
20
15
10
5
0
0.85-0.86
0.87-0.88
0.89-0.9
0.91-0.92
0.93-0.94
0.95-0.96
0.97-0.98
0.99-1
QCDPred probability ranges

Figure 4

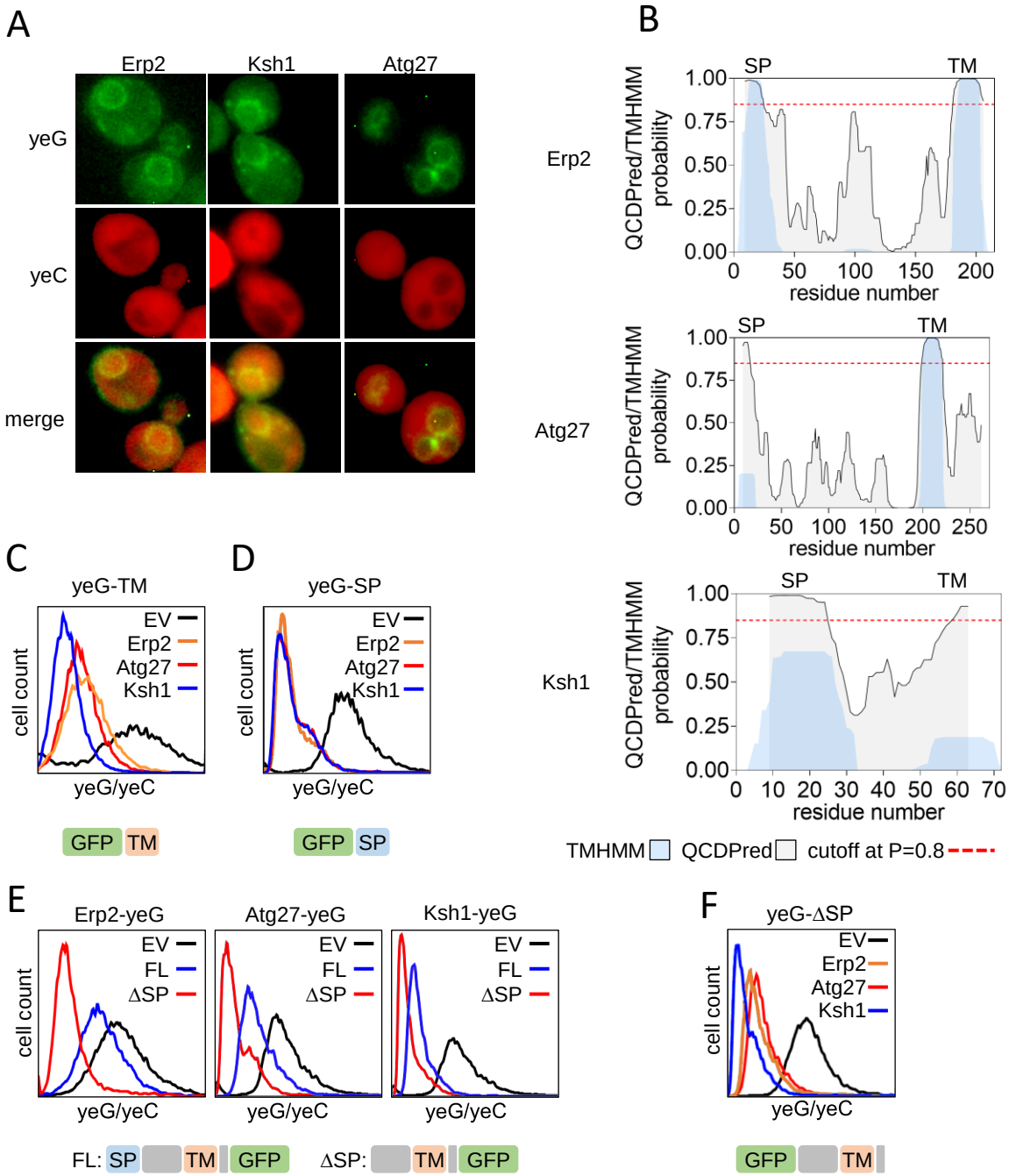
A
Erp2
Ksh1
Atg27
yeG
yeC
merge
B
Erp2
Atg27
Ksh1
SP
TM
QCDPred/TMHMM probability
residue number
TMHMM
QCDPred
cutoff at P=0.8
C
yeG-TM
D
yeG-SP
EV
Erp2
Atg27
Ksh1
cell count
yeG/yeC
GFP
TM
SP
E
Erp2-yeG
Atg27-yeG
Ksh1-yeG
FL
ΔSP
FL:
ΔSP:
F
yeG-ΔSP

Figure 5

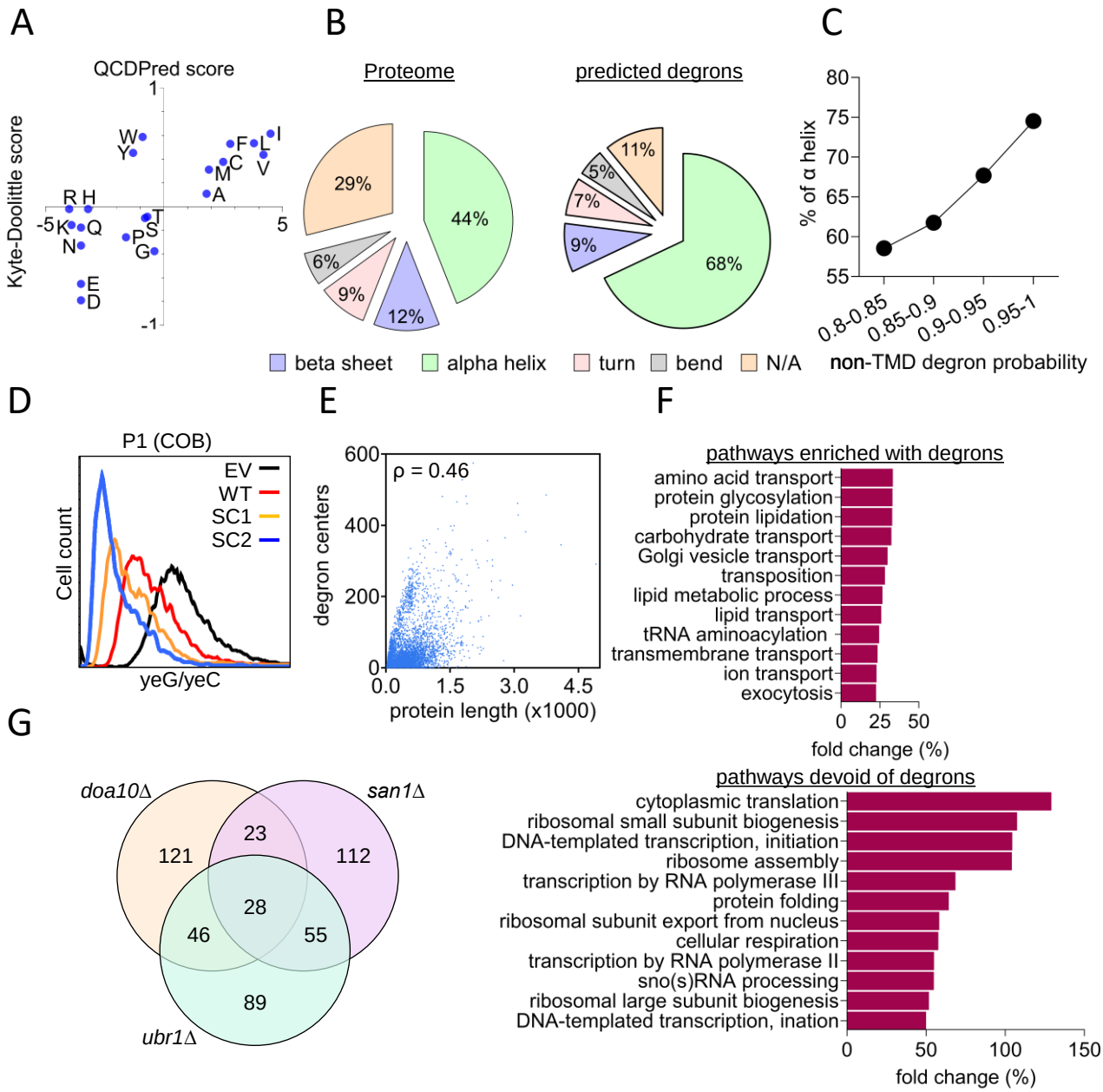
A
QCDPred score
Kyte-Doolittle score
1
-1
-5
5
W
Y
F
L
I
C
M
V
A
R
H
K
Q
N
T
S
P
G
E
D
B
Proteome
predicted degrons
29%
44%
6%
9%
12%
11%
5%
7%
9%
68%
beta sheet
alpha helix
turn
bend
N/A
C
% of α helix
80
75
70
65
60
55
0.8-0.85
0.85-0.9
0.9-0.95
0.95-1
non-TMD degron probability
D
P1 (COB)
EV
WT
SC1
SC2
Cell count
yeG/yeC
E
ρ = 0.46
degron centers
600
400
200
0
0.0
1.5
3.0
4.5
protein length (x1000)
F
pathways enriched with degrons
amino acid transport
protein glycosylation
protein lipidation
carbohydrate transport
Golgi vesicle transport
transposition
lipid metabolic process
lipid transport
tRNA aminoacylation
transmembrane transport
ion transport
exocytosis
0
25
50
fold change (%)
G
doa10Δ
san1Δ
ubr1Δ
121
23
112
28
46
55
89
pathways devoid of degrons
cytoplasmic translation
ribosomal small subunit biogenesis
DNA-templated transcription, initiation
ribosome assembly
transcription by RNA polymerase III
protein folding
ribosomal subunit export from nucleus
cellular respiration
transcription by RNA polymerase II
sno(s)RNA processing
ribosomal large subunit biogenesis
DNA-templated transcription, ination
0
50
100
150
fold change (%)

Figure 6

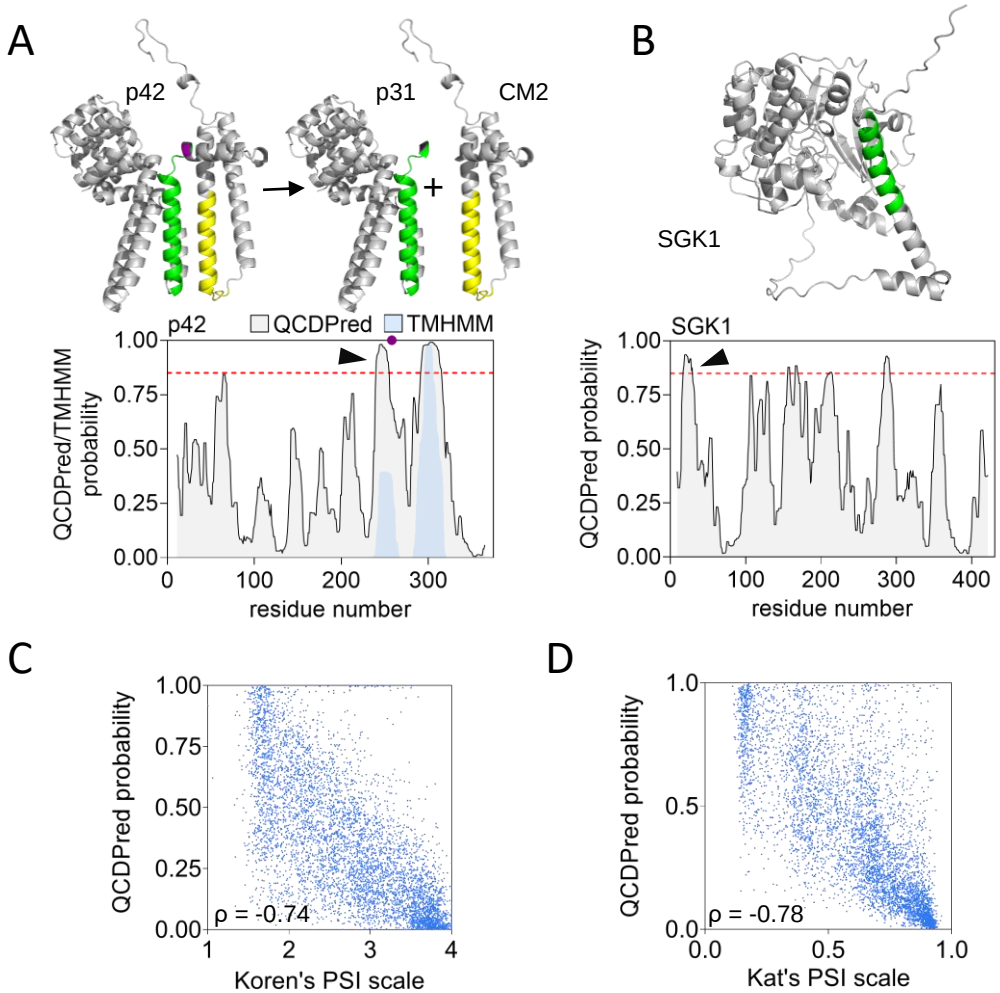
A
p42
p31
CM2
+
p42
QCDPred
TMHMM
QCDPred/TMHMM probability
1.00
0.75
0.50
0.25
0.00
0
100
200
300
residue number
B
SGK1
SGK1
QCDPred probability
1.00
0.75
0.50
0.25
0.00
0
100
200
300
400
residue number
C
QCDPred probability
1.00
0.75
0.50
0.25
0.00
ρ = -0.74
1
2
3
4
Koren's PSI scale
D
QCDPred probability
1.0
0.5
0.0
ρ = -0.78
0.0
0.5
1.0
Kat's PSI scale

Supplemental Figure 1, Isolation of top 10% degrons

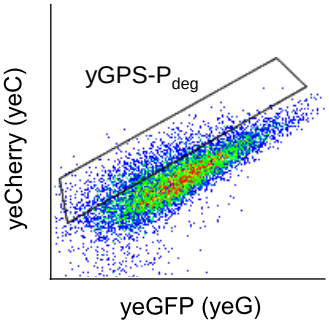

Supplemental Figure 1, related to Figure 1. Isolation of top 10% degrons. Yeast cells expressing yGPS-P_{lib} Were grown to mid-log-phase, followed by FACS of top 10% degron population. One million cells comprising the degron library (yGPS-P_{deg}) were collected, then grown O/N and frozen in liquid nitrogen or taken for further analysis. Illustrated is gating of top 10% degron population out of a total of 10,000 cells.

Supplemental Figure 2

Supplemental Figure 2. **related to Figure 2**. Maps of PSI values emerged from experimental data (black dots), average PSI values for each amino acid (colored in black) and calculated QCDPred probabilities (colored in red) were plotted for each of the proteins in the screen that reach 100% coverage (N=306).

Supplemental Figure 3. Degron prediction in the b-c1 complex

A

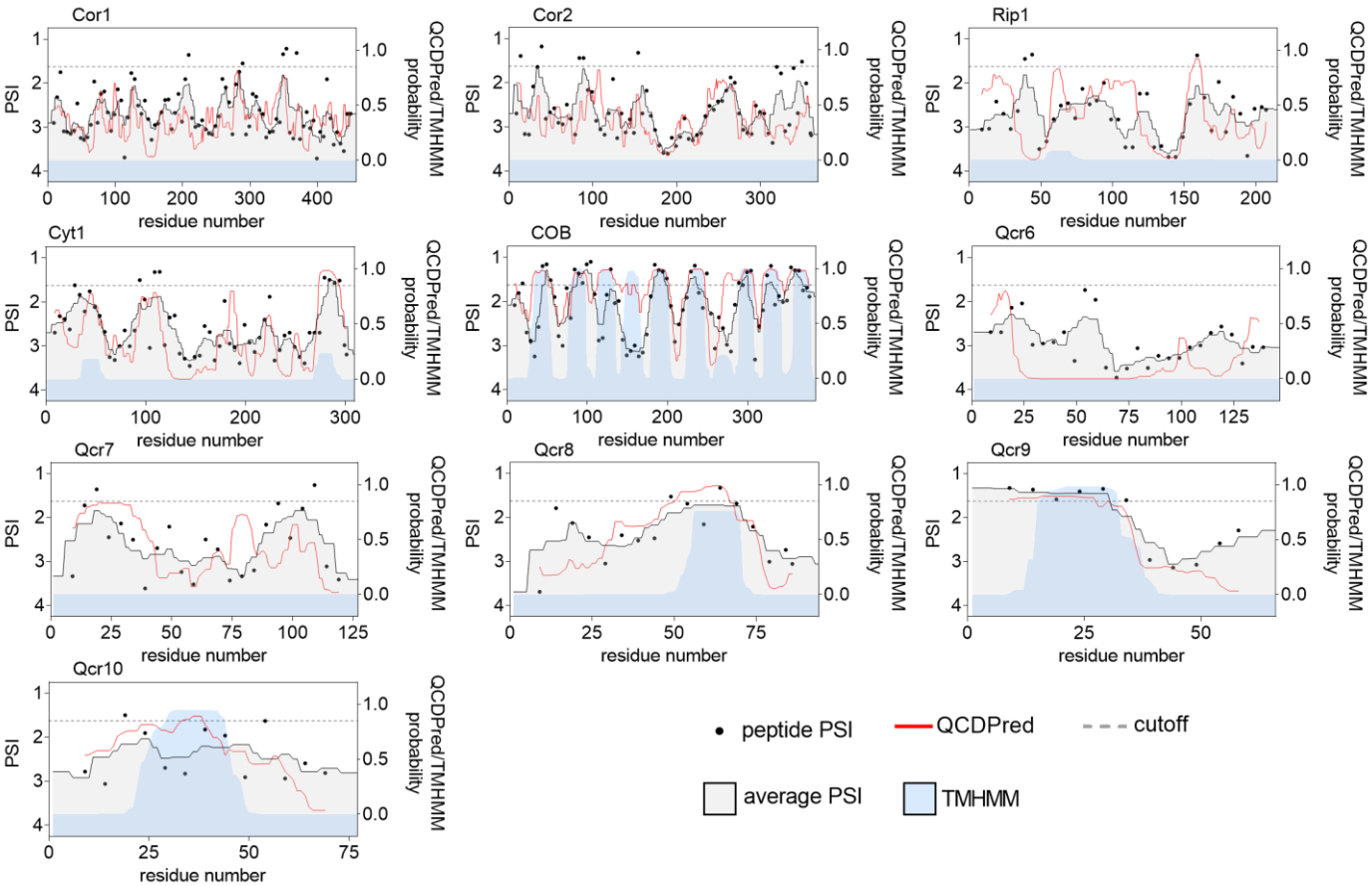

B

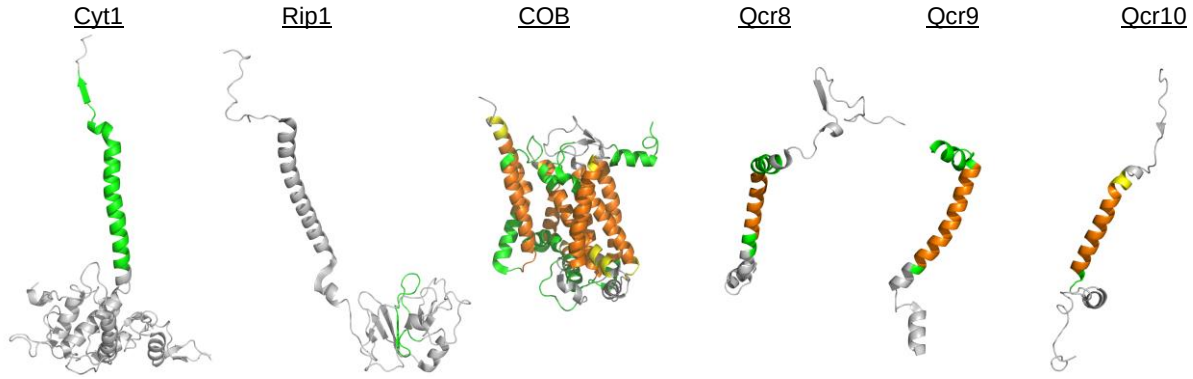

Supplemental Figure 3, related to figure 3. Degrons in the b-c1 complex. (A) PSI values emerged from experimental data (black dots), average PSI values for each amino acid (colored in black), QCDPred probabilities (colored in red), and TMHMM prediction (colored in light blue) were plotted for each subunit of the b-c1 complex. A degron cutoff probability is marked at P = 0.85 by a dashed grey line. (B) Assignment of QCDPred projected Degrons (green) and TMHMM predicted TM domains (yellow) to TM proteins in the b-c1 3D structure (PDB #6t0b). Overlying regions are colored in orange.

Supplemental Figure 4.

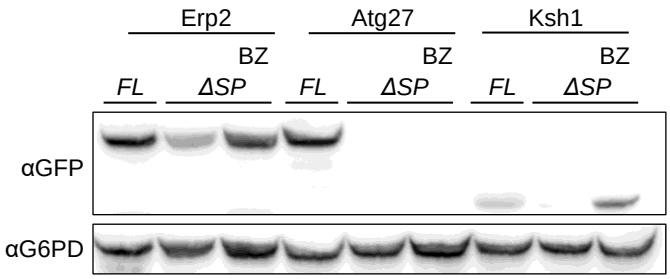

Supplemental Figure 4, related to Figure 4. Immunoblot analysis of Erp2, Atg27 and Ksh1, with or without their SPs. Where indicated, 10 µM of Bortezomib (BZ) were added to cells for 4 hrs prior to cell harvesting. *FL*- full length proteins. Δ*SP*- proteins devoid of the SP. G6PD: Glucose-6-phosphate dehydrogenase

Supplemental Figure 5

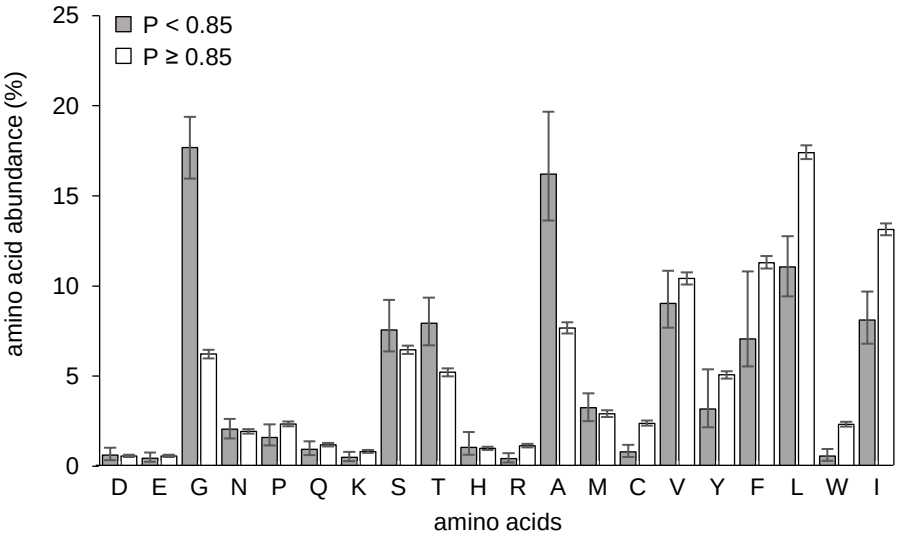

Supplemental Figure 5, Related to Figure 5. Comparison of mean amino acid distribution between TMDs with high degron probability ($P \geq 0.85$, N=6,064) to those with lower probability ($P < 0.85$, N=107). Error bars represent low and high confidence intervals.

Supplemental Figure 6

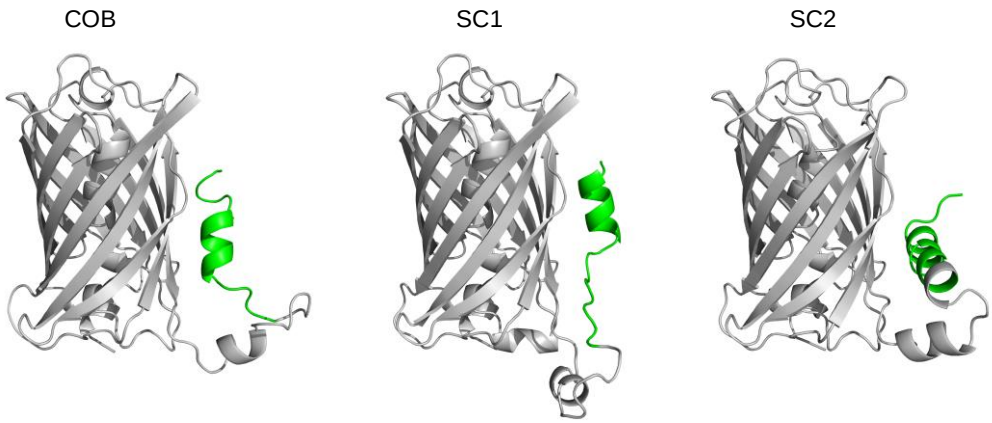

Supplemental Figure 6, related to Figure 5. Structure prediction of GFP-fused peptides using trRosseta. Estimated Template Modeling scores: COB- 0.856, SC1-0.865, SC2-0.828

Supplemental Figure 7

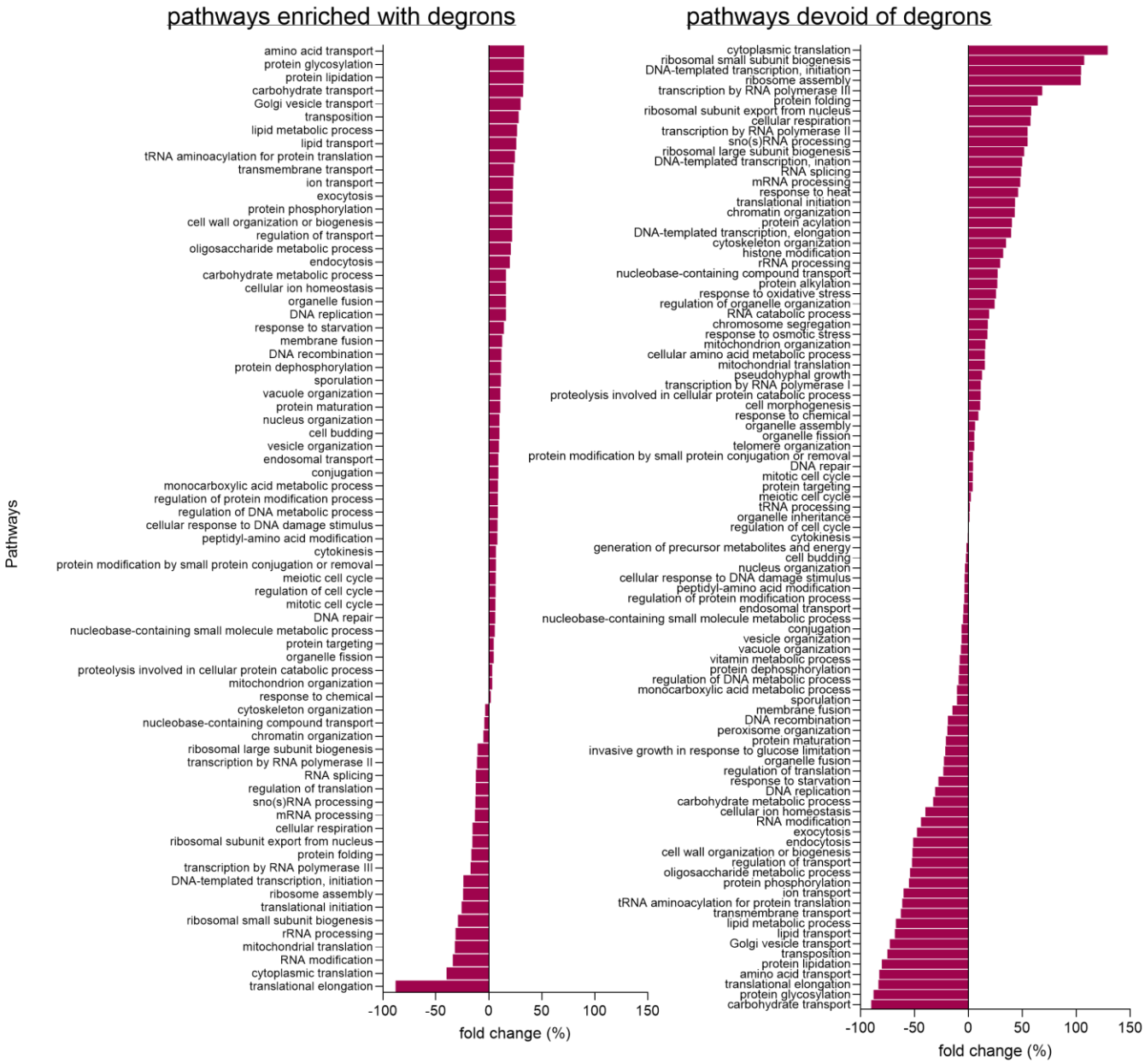

Supplemental Figure 7, related to Figure 5. Large-scale GO annotations of all significant processes (p-value < 0.05) that are either enriched or devoid of predicted degrons at $P \geq 0.85$.

Supplemental Figure 8

Cytosolic/nuclear Hsp40/70 chaperones

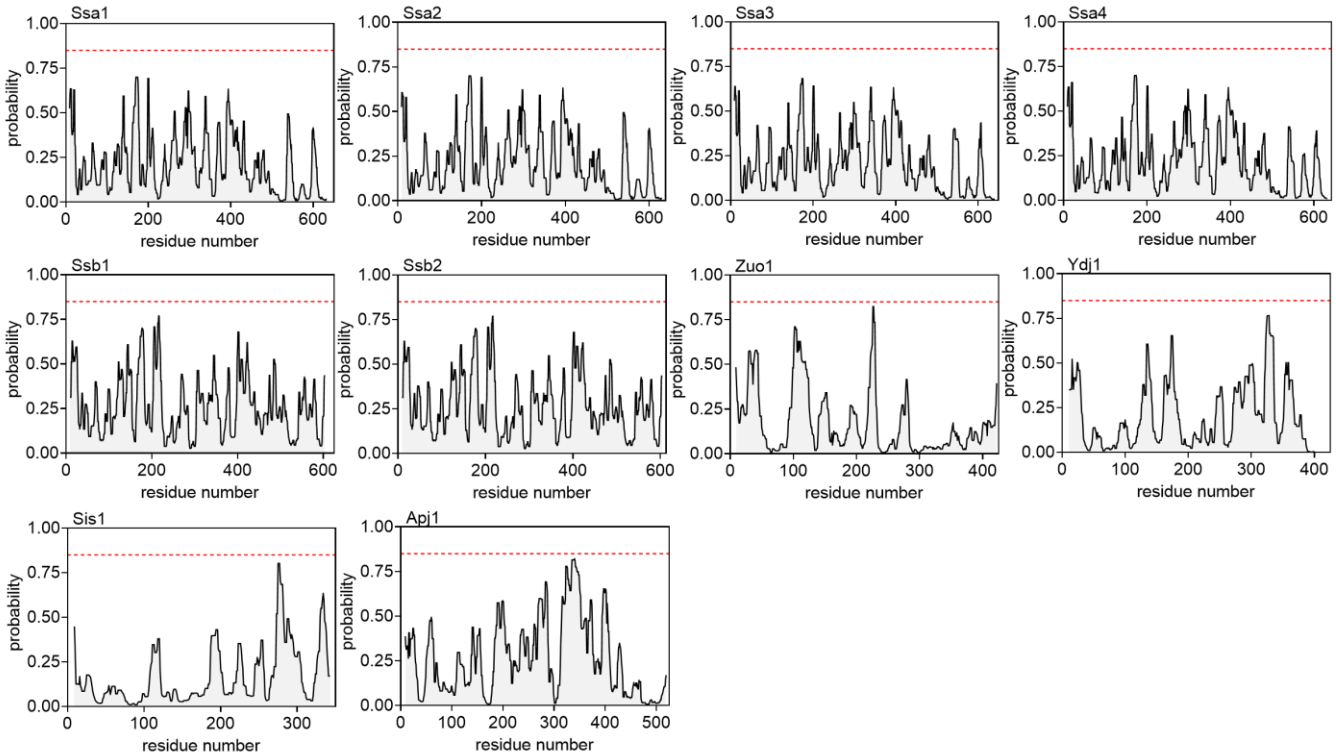

Cytosolic/nuclear Hsp90/100/110 chaperones

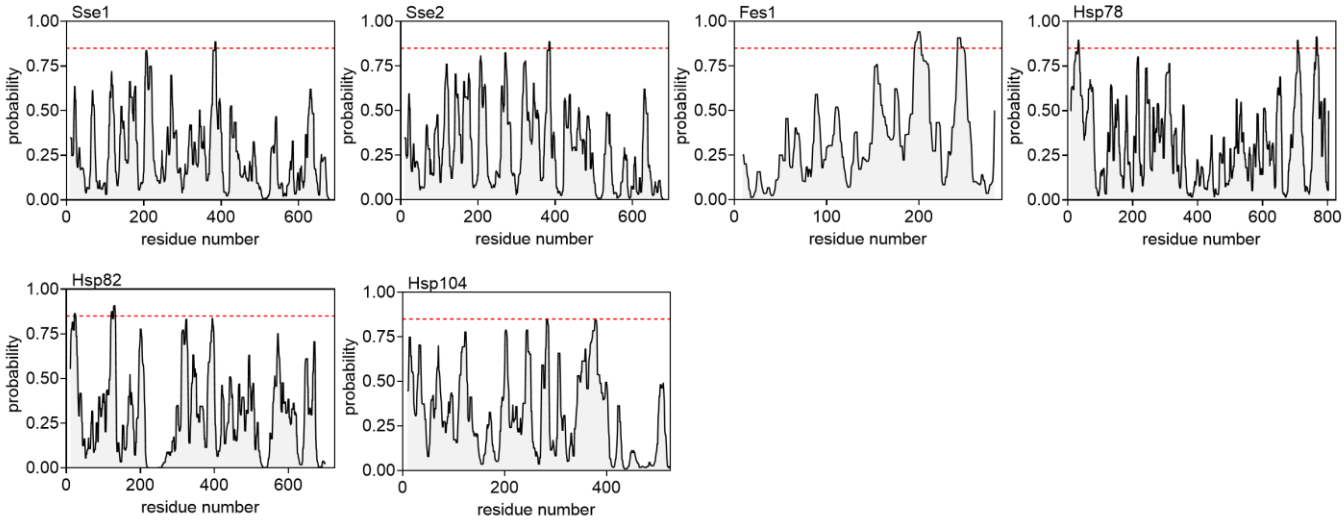

Supplemental Figure 8, related to figure 5. QCDPred probability maps of key cytosolic/nuclear yeast chaperones. A degron cutoff probability is marked at P = 0.85 by a dashed red line.